Mixed rainfall trends highlight the importance of climate adaptation in coastal New South Wales

Authors

Mariam Zachariah, *Centre for Environmental Policy, Imperial College, London, UK*
Kimberley Reid, *School of Geography, Earth and Atmospheric Sciences, The University of Melbourne, Australia*
Andrew King, *School of Geography, Earth and Atmospheric Sciences, The University of Melbourne, Australia*
Pandora Hope, *Bureau of Meteorology, Australia*
Vikki Thompson, *Royal Netherlands Meteorological Institute (KNMI), De Bilt, The Netherlands*
Clair Barnes, *Centre for Environmental Policy, Imperial College, London, UK*
Maja Vahlberg, *Red Cross Red Crescent Climate Centre, The Hague, the Netherlands; Swedish Red Cross, Stockholm, Sweden (based in Ubmeje/Umeå, Sweden)*
Roop Singh, *Red Cross Red Crescent Climate Centre, The Hague, the Netherlands (based in New Jersey, USA)*
Friederike Otto, *Centre for Environmental Policy, Imperial College, London, UK*

Review authors

Joyce Kimutai, *Centre for Environmental Policy, Imperial College, London, UK*
Suzanne Rosier, *Taihoro Nukurangi/National Institute of Water and Atmospheric Research (NIWA), Hataitai, Pōneke/Wellington 6021, Aotearoa New Zealand*
Acacia Pepler, *Bureau of Meteorology, Australia*

Acknowledgments

Daithi Stone*, Taihoro Nukurangi/National Institute of Water and Atmospheric Research (NIWA), Hataitai, Pōneke/Wellington 6021, Aotearoa New Zealand*
Peter Gibson*, Taihoro Nukurangi/National Institute of Water and Atmospheric Research (NIWA), Hataitai, Pōneke/Wellington 6021, Aotearoa New Zealand*

Main findings

- The Mid-North Coast region has several major rivers with low-lying floodplains, and a coastal region housing the major urban centres. This region has endured a series of devastating disasters in recent years, including severe floods and bushfires. Consistent impacts from floods point to the high exposure of people and infrastructure to flooding in this region. The constant cycle of emergencies has left communities grappling with cumulative impacts and recovery fatigue. Rural communities bear the brunt of extreme weather, facing greater property and infrastructure damage, limited access to services, and isolation during disasters.
- A flood watch was issued 3 days in advance of the floods by the Bureau of Meteorology, which allowed for early action to relocate supplies and issue emergency evacuations for highly flood-prone areas, likely reducing impacts.
- Based on gridded data products for the region outlined in Fig. 1, we find that the extreme rainfall event over the study region is relatively common, expected to occur in today's climate only once every 10 years when analysing April to June (AMJ) rainfall, and once every 3 years when considering the whole year. It is important to note the rainfall would have been a rarer and more extreme event in smaller, local regions, and some communities did experience the heaviest rain since records began.
- When comparing the AMJ event today with the same event in a 1.3°C cooler climate, we find a decrease in the likelihood and intensity of extreme rainfall such as observed by about 17%. However, when we look at RX4-day annually we find the event increases with global warming of 1.3°C. The best estimates for the increase in likelihood for the 2025 event associated with this warming is about a doubling, and the increase in intensity for an event of equivalent rarity as observed is about 10%.
- To quantify the role of human-induced climate change in these changes in likelihood and intensity we also analyse climate model data over the study region for the historical period. The models show substantial disagreement, with some projecting significant increases and others indicating decreases in heavy rainfall—both for annual and seasonal RX4-day, as well as when assessing changes in a 1.3°C warmer world. As a result, combining model simulations with observations to obtain an overarching result is not meaningful as different models clearly show changes that are incompatible.
- In addition to examining rainfall totals, we also assess whether the atmospheric circulation patterns driving heavy rainfall have changed over time. We compare an earlier period (1950–1980), when the climate change signal was relatively weak, with a more recent period (1994–2024), marked by a stronger influence of climate change. The analysis shows signs of a seasonal shift—atmospheric circulation patterns that could lead to similar heavy rainfall are now less common in March and more frequent in May. Moreover, present-day events tend to have more rainfall than their historical counterparts. However, not all analogues actually have

rain associated with them and some are not very close analogues, thus rendering it difficult to draw firm conclusions.

- Understanding the influence of climate change on heavy rainfall in the Mid-North Coast is challenging. Consistent with previous studies, our analysis finds no clear trend, as climate models show strong disagreement—some projecting increases, others decreases in heavy rainfall. Observed changes in circulation further suggest that processes beyond the Clausius-Clapeyron relationship are involved. These factors interact in complex ways, and the relatively small size of the region compared to the scale of climate models makes it difficult to assess how these changes manifest within the scope of a rapid study.
- This uncertainty means that both drying and increased rainfall remain possible, so adaptation strategies must be designed to be flexible and responsive to a range of future conditions. Low-regrets adaptation measures that are beneficial in both wet and dry environments, such as nature-based solutions, water storage and diversification measures, and improved risk management can be useful options.

1 Introduction

Heavy rains from May 19-23 led to large scale flooding in New South Wales (NSW). On each of these days areas along the New South Wales coast received more than 100 mm of rain with especially high rainfall totals on the Mid North Coast, including the cities of Newcastle, Taree and Port Macquarie. In total, the resulting floods killed five people, 700 needed to be rescued and 50,000 people were stranded during and in the immediate aftermath of the event (Sky News, 2025). Thousands of homes sustained damage, with close to 800 deemed uninhabitable (The Guardian, 2025). While the full scale of damages will only be known in the weeks and months after the event, it is clear that farmers were particularly hard hit, many losing their herds and others the means to feed their cattle (ABC News 2025). Prior to the event, severe weather warnings for heavy rainfall and damaging winds were in place for the Hunter and Mid North Coast. The State Emergency Services (SES) and National Emergency Management Authority (NEMA) were informed by the Bureau of Meteorology (Bureau) of the forecast storm, rain and flood risk at least seven days prior, with increasing detail in the lead-up. Hazard warnings were shared with the public via the Bureau's website, app and media channels (e.g., X|BoM NSW).

The extreme rainfall was associated with persistent high pressure to the southeast in the Tasman Sea blocking the westerly atmospheric flow and advecting moist air from the ocean over the coast. Two upper-level cyclones, that ultimately merged, provided persistent uplift for the moist air. This setup enhanced moisture advection and ascent ultimately increasing the rainfall totals. This dynamic setup is typical during extreme rainfall events in this region (Holgate et al, 2023). However, the duration of this event was unusual. The duration of high pressure systems in the Tasman Sea is typically one-two days (Reid et al, 2025) whereas this event lasted four days. A similar synoptic pattern occurred in March 2021, which also caused significant flooding in this region (Reid et al, 2021).

1.1 Review of attribution studies on previous heavy rainfall events in the region

Several attribution studies on the role of human-induced climate change on heavy rainfall in Australia have been published. Most of these did not find a discernible influence. Analysing extreme rainfall in 2011/2012 over southeastern Australia, King et al., (2013) found limited evidence for a role of climate change, but did not exclude that it may have played a role. Similarly, Christidis et al., (2013) concluded that heavy rains in Eastern Australia in March 2012 were driven by natural variability, as did Hope et al., (2018) for extreme rainfall in September 2016 in South East Australia and King et al., (2018) studying the record wet winter 2016 in the same region. In a study assessing the 1-day extreme precipitation in Tasmania in May 2018 the authors concluded that there is insufficient evidence to draw a conclusion but that for “moderate magnitude Hobart daily rainfall extremes, models suggest that the associated extratropical lows will deliver more rainfall with weaker pressure anomalies in a warmer world” (Tozer et al., 2020). Hirabayashi et al. (2021) even found that climate change made river flooding of the Fitzroy river in 2010 less likely, while the same study focussing on the Murray and Murrumbidgee river flooding in 2012 found again no discernible influence. Dittus et al., (2017) assessed several extreme rainfall indices over all of Australia, analysing trends between 1951 and 2005 and found no attributable trends in heavy rainfall indices. Similar to these studies from comparably long-ago events, even the more recent events are proving to be difficult to assess from a climate change point of view. Cadiou et al., (2023) found in an observations-based study on heavy rainfall in February and March 2022 that no clear statement with respect to the role of climate change can be made due to the influence of La Niña and the uniqueness of that particular event.

While most studies have focussed on daily-to-multi day extreme rainfall changes, limited analysis of sub-daily and sub-hourly rainfall extremes (Guerreiro et al., 2018, Osburn et al. 2021; Wasko et al. 2024), including a study specifically focussed on coastal New South Wales (Ayat et al. 2022), suggests that on these timescales extreme rainfall intensification is detectable. Attribution analyses on short-duration, localised extreme rain events are more challenging than larger-scale, longer events, but given the detectability of stronger trends and understanding of climate change effects on thermodynamics, would be expected to exhibit stronger anthropogenic influences.

Studies of future projections suggest that there may be a decrease in the frequency of the synoptic conditions that led to this event. Projections of blocking highs in the Tasman Sea are uncertain although models generally indicate a reduction in blocking under anthropogenic warming (Patterson et al, 2019). The frequency of upper-level lows over New South Wales is projected to decrease (Pepler and Dowdy, 2021) and therefore the combined Tasman high-upper low pattern, which is conducive to extreme rainfall, is expected to decline (Holgate et al, 2023). However, the amount of moisture available and rainfall generated during the most intense of these events may increase, leading to potential increases in the frequency of rare high-impact events (Pepler & Dowdy 2022, Reid et al. 2021)

1.2 Event Definition

For this study, we focus on the region within the orange alert zone along the coast of New South Wales, spanning from 37.5°S to 29°S. To exclude the mountainous areas, the western boundary is defined by the edge of the southeast coastal river drainage basin. This coastal region not only experienced the highest rainfall and associated impacts during the event but is also climatologically homogeneous. The region is outlined in red in Figure 1.1. For the temporal event definition we focus on the four days with heaviest rainfall (Rx4day). We have tested the sensitivity of the event definition for longer duration (RX7day) and only the region of the most impacts (north of 34°S) and found that while the exact return times of course differ, the trends are comparable. We thus focus on the days of the heaviest rainfall and the climatologically homogenous region of the orange alert zone. Figure 1.1 shows the total rainfall during 19-22 May 2025, in three gridded datasets- ERA5, MSWEP and CPC (details of these datasets are provided in Section 2.1).

The selected study area incidentally falls in a transition region, both geographically and climatically. The region to the south of the domain exhibits a clear drying trend associated with climate change in the colder months of the year, while regions to the north, tend to have mixed trends in rainfall. Additionally, the timing of the event—May—coincides with a seasonal transition from the warmer to the cooler part of the year. To capture both the spatial and temporal complexity of these features, we use two event definitions: one focusing on the season centered around May (April to June, AMJ), and another considering the wettest four days of the year (running from July of previous year to June) irrespective of season. The annual definition is motivated by the historical record, which showed that extreme rainfall and flooding events in the region have previously been driven by meteorological processes comparable to those associated with the event under study, and such events can occur at any time of year.

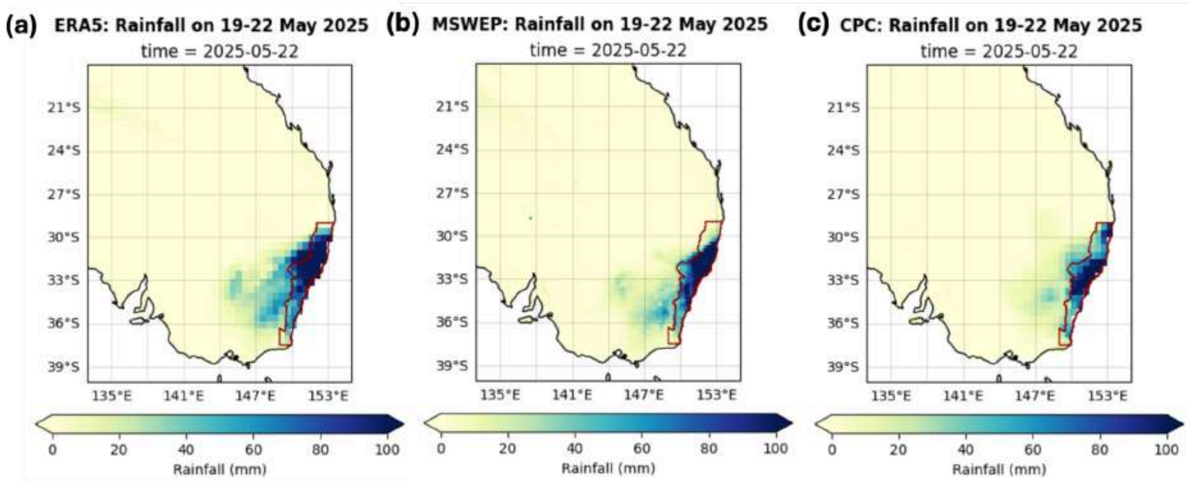

Figure 1.1: *4-day accumulated rainfall during 19-22 March 2025, based on (a) ERA5 (b) MSWEP and (c) CPC data. The study region is highlighted in red.*

In this report, we study the influence of anthropogenic climate change by comparing the likelihood and intensity of similar Rx4day events in the current climate with those in a 1.3 °C cooler climate. We also extend this analysis into the future by assessing the influence of a further 1.3 °C of global warming from present. This is in line with the latest Emissions Gap Report from the United Nations Environment Programme, which shows that the world is on track for at least 2.6 °C temperature rise given currently implemented policies (UNEP, 2024).

2 Data and methods

2.1 Observational data

We utilise daily data for four gridded observational datasets and two in situ stations :

1. **ERA5 (5th Generation product from the European Centre for Medium-Range Weather Forecasts (ECMWF)**. ERA5 reanalysis product begins in the year 1950 (Hersbach et al., 2020). We use daily rainfall from this product. It should be noted that the variables from ERA5 are not directly assimilated, but these are generated by atmospheric components of the Integrated Forecast System (IFS) modelling system. Due its low performance in the

pre-satellite period, we utilised only data from 1983 onwards from this dataset. At the time of analysis, reanalysis data were available through the end of April 2025, analysis data covered the first 22 days of May, and forecast data were used for the period 23–27 May.

2. **Multi-Source Weighted-Ensemble Precipitation (MSWEP).** MSWEP v2.8 dataset (updated from Beck et al., 2019) is fully global, with precipitation available at 3-hourly intervals and at 0.1° spatial resolution, available from 1979 to ~3 hours from real-time. This product combines gauge-, satellite-, and reanalysis-based data.
3. **CPC**- This is the gridded product from NOAA PSL, Boulder, Colorado, USA known as the CPC Global Unified Daily Gridded data, available at 0.5° x 0.5° resolution, for the period 1979-present. Data are available from NOAA. We use daily precipitation from this product.
4. **Weather Station data**. We employ the Australian Gridded Climate Dataset version 1 (AGCDv1), formerly referred to as AWAP, which provides daily gridded rainfall data across the Australian continent at a spatial resolution of 5 km. The dataset is constructed through interpolation of station-based observations and spans the period from 1900 to the present (Jones et al. 2009). Although AGCDv1 is considered highly reliable for large-scale rainfall analysis, previous studies have indicated that it may underrepresent certain localised extreme rainfall events (King et al., 2012), similar to other gridded products.

As a measure of anthropogenic climate change we use the (low-pass filtered) global mean surface temperature (GMST), where GMST is taken from the National Aeronautics and Space Administration (NASA) Goddard Institute for Space Science (GISS) surface temperature analysis (GISTEMP, Hansen et al., 2010 and Lenssen et al. 2019).

2.2 Model and experiment descriptions

We use five multi-model ensembles from climate modelling experiments using very different framings (Philip et al., 2020): Sea Surface temperature (SST) driven global circulation high resolution models, coupled global circulation models and regional climate models.

1. **Coordinated Regional Climate Downscaling Experiment (CORDEX)**-Australasia(0.44° resolution, AUS-44 and 0.22° resolution, AUS-22) multi-model ensemble (Virgilio et al., 2019). We use 5 sets of simulations resulting from pairings of four Global Climate Models (GCMs) and two Regional Climate Models (RCMs). These simulations are composed of historical simulations up to 2005, and extended to the year 2100 using the RCP8.5 scenario.

2. **HighResMIP** SST-forced model ensemble (Haarsma et al. 2016), the simulations for which span from 1950 to 2050. The SST and sea ice forcings for the period 1950-2014 are obtained from the 0.25° x 0.25° Hadley Centre Global Sea Ice and Sea Surface Temperature dataset that have undergone area-weighted regridding to match the climate model resolution. For the 'future' time period (2015-2050), SST/sea-ice data are derived from RCP8.5 (CMIP5) data, and combined with greenhouse gas forcings from SSP5-8.5 (CMIP6) simulations (see Section 3.3 of Haarsma et al. 2016 for further details).

3. **Conformal Cubic Atmospheric Model (CCAM)** is a high-resolution, non-hydrostatic global climate model developed in Australia to simulate atmospheric processes with fine spatial detail (Thatcher and McGregor 2009). In the configuration used here it employs a

variable-resolution grid that decreases in resolution as a function of distance from Aotearoa New Zealand. Over eastern Australia the resolution of the numerical calculations is about 15 km, but the output is interpolated to an approximately 35 km grid. Ten members of a perturbed initial-condition ensemble for the historical period 1982–2021, or the historical experiment (i.e., the factual scenario) that mimics the CMIP6 historical scenario forcings, but with the boundary SST conditions prescribed from observations across years 1982–2021, naturalised (counterfactual) runs in which anthropogenic influences are removed (through modification of greenhouse gas, aerosol, and ozone concentrations and adjustment of the SSTs according to a CMIP6-based estimate), and future climate projections representing a world 2°C warmer than pre-industrial (through similar modifications as the naturalised runs, but only covering 2009-2021) are used in this study (Gibson et al., 2023; Stone et al., 2024).

4. **Bias-adjusted CORDEX-CMIP6 models** This set comprises of a set of downscaled CMIP6 models contributed by CSIRO and the Bureau of Meteorology to the CORDEX-CMIP6 project using the BARPA-R and CCAM RCMs (Howard et al., 2024; Schroeter et al., 2024; CSIRO and Bureau of Meteorology, 2025). The precipitation data has been bias corrected against the Australian Gridded Climate Dataset (AGCD) using Quantile Matching for Extremes (QME; Dowdy 2023). Simulations for Historical and the SSP3-7.0 scenarios from 14 models are used in this study.

5. **weather@home/ANZ** (Black et al. 2016, Massey et al. 2015) runs the UKMO global model HadAM3P at resolution 1.875lat x 1.25long (ca. 150km) with the regional model HadRM3P over the Australasian CORDEX domain, at 0.44deg (ca. 50km) resolution, nested inside it. Both models are quasi-hydrostatic and atmosphere-only, and via public distributed computing multi-thousand member ensembles are created. For this study, four sets of simulations were supplied: a 'current decade' (actually mid-2006 to mid-2016), which uses SSTs and sea ice from the UKMO 'OSTIA' dataset (Donlon et al. 2012) and an end-of-century decade under each of three futures: +1.5, +2 and +3degC warmer than pre-industrial . These were set up according to the 'HAPPI' framework (Mitchell et al. 2017), via adjustment of GHGs, aerosol and ozone radiative forcings and SSTs and sea ice to end-of-century conditions. Each of the four datasets consists of ca. 2500-3200 simulations. .

2.3 Statistical methods

Methods for observational and model analysis and for model evaluation and synthesis are used according to the World Weather Attribution Protocol, described in Philip et al., (2020), with supporting details found in van Oldenborgh et al., (2021), Ciavarella et al., (2021), Otto et al., (2024) and here. The key steps, presented in sections 3-6, are: (3) trend estimation from observations; (4) model validation; (5) multi-method multi-model attribution; and (6) synthesis of the attribution statement.

In this report we analyse time series of (1) annual (July-June) Rx4day and (2) AMJ Rx4day. Non-stationary Generalised Extreme Variable (GEV) distributions are used to model them. The distribution is assumed to scale exponentially with the covariates, with the dispersion (the ratio between the standard deviation and the mean) remaining constant over time; while for temperatures, the distribution is assumed to shift linearly with the covariates, while the variance remains constant. The parameters of the statistical model are estimated using maximum likelihood.

For each time series we calculate the return period and intensity of the event under study for the 2024 GMST and for 1.3 °C cooler GMST: this allows us to compare the climate of now and of the preindustrial past (1850-1900, based on the Global Warming Index), by calculating the probability ratio (PR; the factor-change in the event's probability) and change in intensity of the event.

2.3.1 Exceptions in methods

In addition to the primary method described in Section 2.3, which applies to observational data and model runs with transient forcing (HighResMIP and COREDEX models, as well as considering only the all-hist runs in from CCAM ensemble), the return periods and risk ratios are estimated directly between two different scenarios- all hist/current decade vs. naturalised runs, and all hist vs. 2 °C warmer world, for the weather@home and CCAM models. Examples of past attribution studies that use this approach include Stone et al. (2024a), Philip et al. (2018) and Otto et al. (2018).

3 Observational analysis: return period and trend

3.1 Analysis of gridded data

Table 3.1 summarises the magnitude of the extreme rainfall event of May 2025, area-averaged over the study region, when considering the annual (Jun-July) maxima as well as the seasonal (AMJ) maxima, along with their respective estimated return periods in the 2025 climate.

Considering the annual (Jul-Jun) RX4day event in the four gridded datasets- AWAP, ERA5, MSWEP, and CPC (see Section 2.1 for details of the datasets), we find the magnitude of the 2025 event to be comparable in all datasets except CPC, which recorded a lower value of about 73.4mm of rain during the four days of heaviest rainfall, as compared to 90-110mm recorded in the other datasets. The 2025 annual event is not rare, with a recurrence interval of 1-in-1 to 1-in-3 year in the different datasets. The AWAP dataset which is a high-resolution gridded dataset obtained by interpolation of observed station records has the longest length of daily observed rainfall records beginning in the year 1900, and therefore it is reasonable to treat this dataset as a close representation of observed reality, and as a baseline for evaluating the other gridded datasets. The closeness in the estimated magnitude and the rarity of the 2025 event among the other datasets to those from the AWAP dataset, attests to the performance of the gridded reanalysis products over this region. Considering the 2025 event as the seasonal (AMJ) extreme, the event has a return period ranging from 5 to 14 years between the different datasets. For the attribution analysis, we round these values and define the 2025 rx4day event as a 1-in-3 year event for the annual (Jul-Jun) case, and a 1-in-10 year event when considering the event in the context of the AMJ season. It is important to note that these return periods arrived at from analysing the observed datasets correspond to the slightly bigger region that includes the areas most heavily impacted by the event. As such, they should not be interpreted as evidence that the observed data failed to capture the extremeness of the rainfall. In fact, the rainfall would have been even rarer and more extreme in smaller, localized areas, where some communities experienced the heaviest rainfall since records began.

Table 3.1: *Estimated return periods of the 2025 event when defined as annual (Jul-Jun) Rx4day and Seasonal (AMJ) Rx4day events over the study region in the four reanalysis and station-interpolated datasets with coverage of the event.*

Dataset	Annual (Jul-Jun) rx4day		AMJ rx4day	
	Magnitude (mm/4day)	Return period (95% C.I.)	Magnitude (mm/4day)	Return period (95% C.I.)
AWAP	109.01	2.226 (1.519 ... 3.901)	109.01	10.245 (4.031 ... 43.044)
ERA5	92.855	2.634 (1.623 ... 6.08)	92.855	13.839 (3.943 ... 204.432)
MSWEP	99.31	2.203 (1.198 ... 4.925)	99.31	9.05 (2.874 ... 81.753)
CPC	73.435	1.222 (1.046 ... 1.893)	73.435	5.18 (2.284 ... 27.19)

Figures 3.1 -3.2 show the trend fitting methods described in Section 2.3 applied to the annual (Jul-June) and seasonal (AMJ) Rx4day events, area-averaged over the study region based on AWAP, ERA5, MSWEP and CPC datasets.. The left panels in these figures show the variable as a function of the GMST anomaly, while the right panels show the GEV distribution-based return period curves for this variable in the present 2025 climate (red lines) and the past climate when the global mean temperature was 1.3°C cooler (blue lines) for the respective datasets.

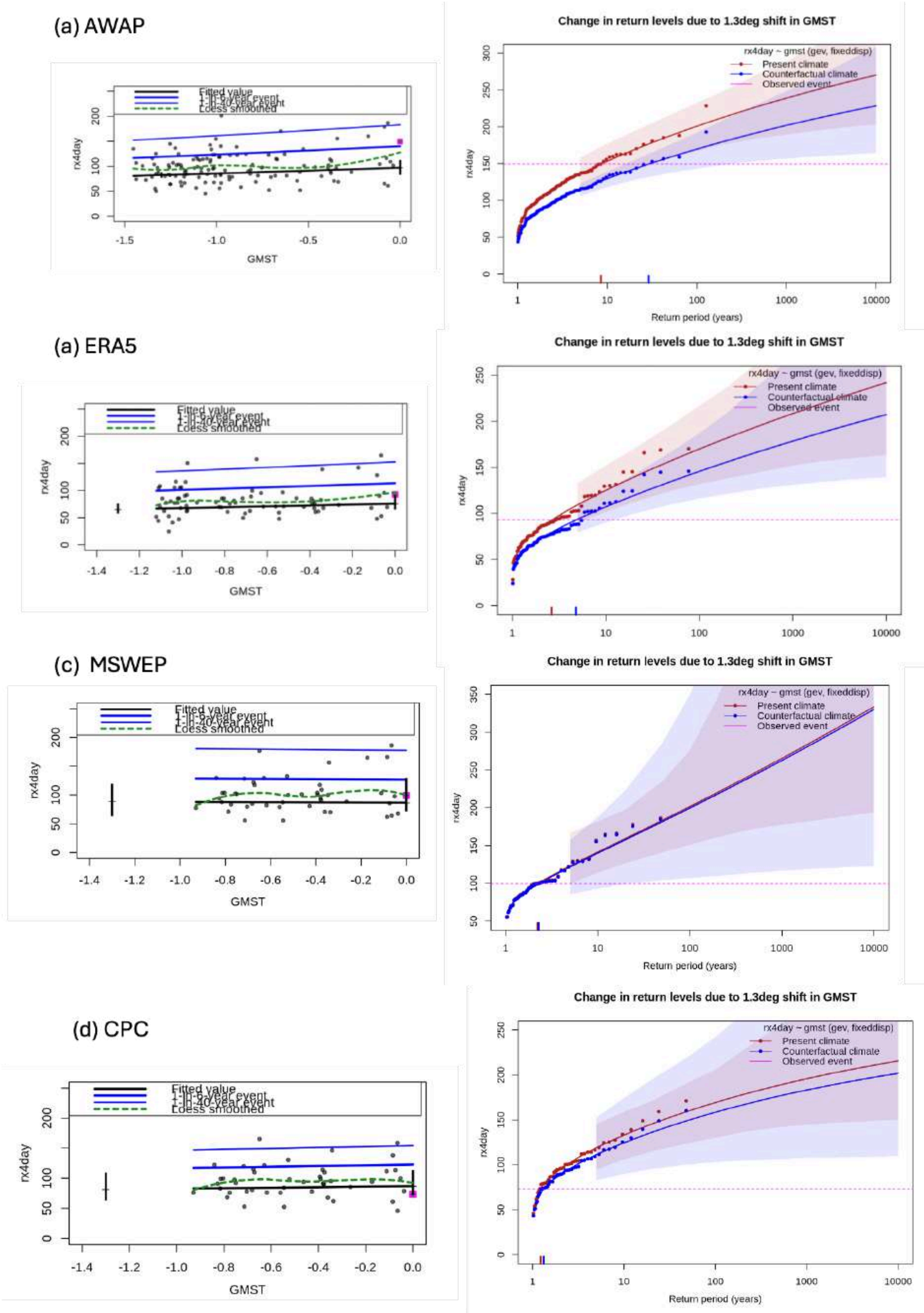

Figure 3.1: *GEV fit with fixed dispersion and location parameter scaling proportional to GMST of the index series.* ***(left)*** *Observed annual (Jul-June) max.4-day cumulative rainfall [mm/4day] as a*

function of the smoothed GMST. The thick black line denotes the time-varying location parameter. The vertical black lines show the 95% confidence interval for the location parameter, for the current, 2025 climate and the fictional, 1.3ºC cooler climate. The 2025 observation is highlighted with the magenta box. ***(right)*** *Return time plots for the climate of 2025 (red) and a climate with GMST 1.3 ºC cooler (blue). The past observations are shown twice: once shifted up to the current climate and once shifted down to the climate of the pre-industrial era. The markers show the data and the lines show the fits and uncertainty from the bootstrap. The magenta line shows the magnitude of the 2025 event analysed here. These are shown for (a) AWAP (b) ERA5, (c) MSWEP and (d) CPC.*

(a) AWAP

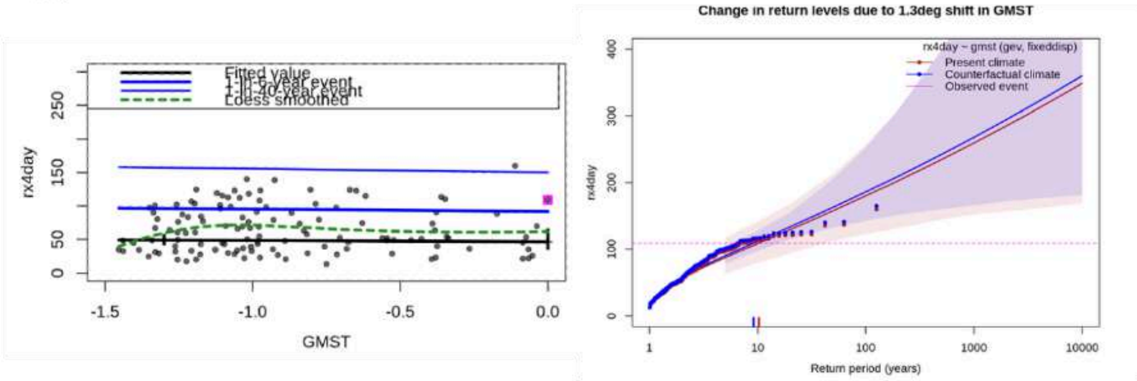

(a) ERA5

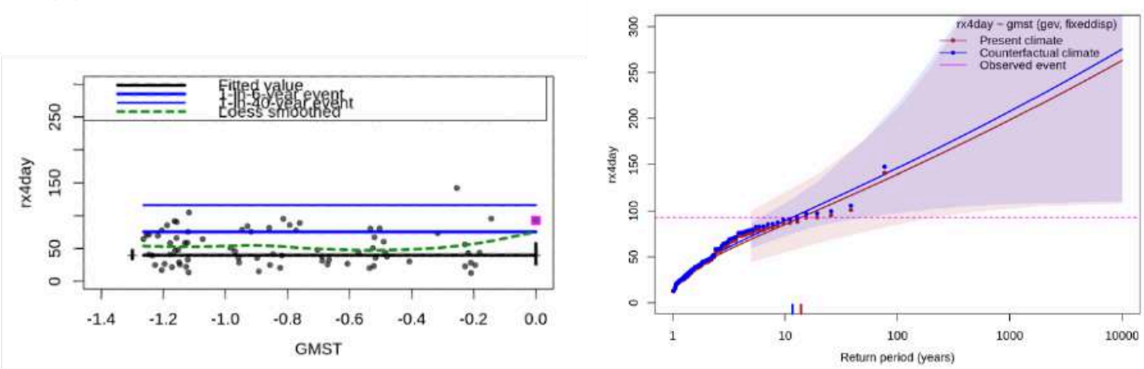

(c) MSWEP

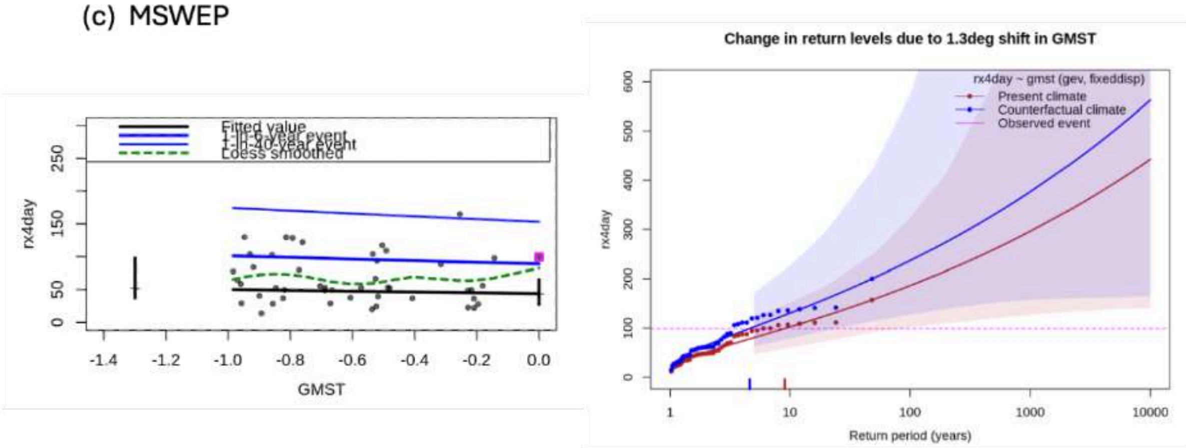

(d) CPC

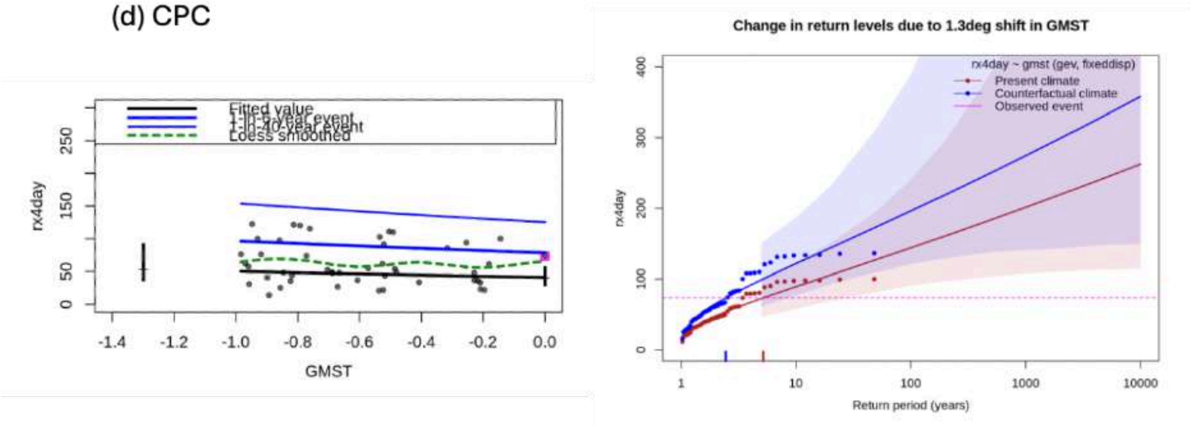

Figure 3.2: *GEV fit with fixed dispersion and location parameter scaling proportional to GMST of the index series.* ***(left)*** *Observed seasonal (AMJ) max.4-day cumulative rainfall [mm/4day] as a function of the smoothed GMST. The thick black line denotes the time-varying location parameter. The vertical black lines show the 95% confidence interval for the location parameter, for the current, 2025 climate and the fictional, 1.3ºC cooler climate. The 2025 observation is highlighted with the magenta box.* ***(right)*** *Return time plots for the climate of 2025 (red) and a climate with GMST 1.3 ºC cooler (blue). The past observations are shown twice: once shifted up to the current climate and once shifted down to the climate of the pre-industrial era. The markers show the data and the lines show the fits and uncertainty from the bootstrap. The magenta line shows the magnitude of the 2025 event analysed here. These are shown for (a) AWAP (b) ERA5, (c) MSWEP and (d) CPC.*

Considering the annual definition, Rx4day events are seen to become heavier due to rising global temperatures. This signal is consistent across all datasets (left panels in Fig. 3.1). Consequently, the best estimated PR is greater than 1 in all datasets suggesting that rainfall extremes such as the 2025 event are more common in today's climate as compared to the 1.3 °C climate. The intensity changes suggest that such extremes have been made up to 16% more intense due to human-induced climate change. We note that these values are not statistically significant (see Table 3.1 for the uncertainty bounds). However, this is unsurprising and consistent with documented trends in extreme rainfall in the region which show an increasing tendency driven by thermodynamic factors, which are prevalent in the austral summer when the rainfall extremes tend to occur more. Contrary to this, the AMJ rx4day is found to display decreasing tendency associated with global warming, again characteristic of the increase in mean sea level pressure during the austral winter, which strengthens the subtropical ridge, thereby decreasing the rain from extratropical weather systems like lows and fronts (BoM, 2024). Consequently, the best estimated PR suggests decrease in the likelihood of the event in today's climate as compared to the 1.3 °C cooler climate, along with a 3 to 27% reduction in the magnitude of the rainfall.

Table 3.2: *Change in probability ratio and magnitude for the 2025 event when defined as annual (Jul-Jun) Rx4day and Seasonal (AMJ) Rx4day, due to GMST.. Light blue indicates an increasing trend that crosses no change, while light orange indicates a decreasing trend. Statistically significant trends are also highlighted in* ***bold*** *font.*

Dataset	Annual (Jul-Jun) rx4day		AMJ rx4day	
	Probability Ratio	Change in magnitude (%)	Probability Ratio	Change in magnitude (%)
AWAP	1.7 (0.84 ... 3.3)	16 (-4.2 ... 39)	0.89 (0.16 ... 3.4)	-3.2 (-35 ... 40)
ERA5	1.8 (0.50 ... 6.6)	17 (-15 ... 60)	0.84 (0.039 ... 8.4)	-4.5 (-45 ... 58)
MSWEP	1.0 (0.26 ... 17)	1.0 (-34 ... 90)	0.51 (0.024 ... 6.5)	-21 (-71 ... 79)
CPC	1.1 (0.56 ... 2.4)	6.8 (-36 ... 68)	0.47 (0.051 ... 2.9)	-27 (-68 ... 50)

3.3 Circulation Analogues

3.3.1 Data and methods

Atmospheric flow analogues can be used to assess changes in the intensity of dynamically similar events or changes in the frequency of occurrence of particular circulation patterns (Cattiaux et al., 2010; Vautard et al., 2016; Jézéquel et al., 2018, Thompson et al 2024). Here we use ERA5 data to assess analogues identified from 500 hPa geopotential height (Z500) since 1950, to detect trends in the frequency of circulation patterns similar to those associated with the heavy rainfall event.

To identify the most similar events, we compute the Euclidean distance between the Z500 anomaly field of the 20th May 2025 and every other day (1950–2024) over the region bounded by [140° to 160°E, 25° to 40°S]. To avoid double-counting persistent events, the identified events must be separated by at least 5 days. The region and circulation variable were determined by assessing the event itself, and earlier current understanding of the circulation drivers of similar events (Holgate et al 2023).

To determine potential shifts in seasonality, and which months to include in further assessment, we identify the top 0.5% of days annually for two periods. We select an early period (1950-1980), defined by weaker climate change signal and a later period (1994-2024), characterised by a stronger climate change signal. We identify the 60 closest analogue days within each period, and determine the month in which they occur (Fig.2.3). As the event occured in May, yet there are very few June analogues, we choose to use MAM in the rest of the analogue assessment.

To detect trends in the circulation pattern and intensity since 1950 we identify the closest 29 analogues across the two periods (1950-1980 and 1994-2024). This corresponds to the closest 1% of days in each period. The average weather conditions associated with the two sets of analogues - called 'composites' - are then compared to assess differences between the two periods We also assess the change in frequency of the closest analogues through time. This is assessed at three different thresholds - the upper 5% of days, upper 10%, and upper 20%. Differences in modes of internal variability between the two time periods can also induce differences in the weather conditions, therefore we cannot identify the role of climate change solely by comparing analogue sets in reanalyses.

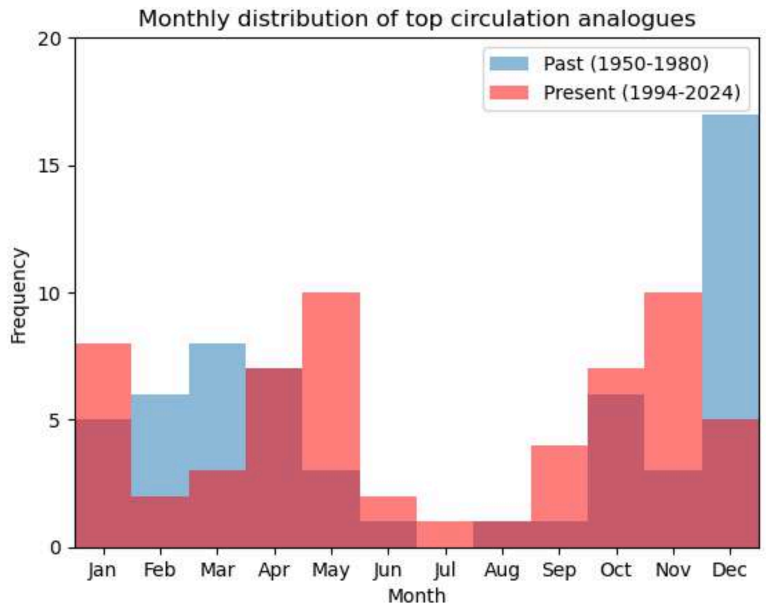

Figure 3.3 *Monthly distribution of the closest analogues. Showing the number of analogues within the closest 0.5% annually (60 events per period) occurring in each month for a past period (1950-1980) and a present period (1994-2024).*

3.3.2 Results

On 20th May 2025 a persistent high pressure system lay to the southeast of the extreme rainfall whilst a low pressure system lay to the northwest, depicted in Fig. 3.4 This dynamic setup is typical during extreme rainfall events in this region (Holgate et al, 2023). A similar synoptic pattern occurred in March 2021, which also caused significant flooding in this region (Reid et al, 2021).

We show how events showing similar atmospheric circulation patterns have changed in the present (1994–2024) compared to the past (1950–1980). Assessing the most similar 0.5% of days within the two periods we see that the circulation pattern is very unusual in June-September (Fig. 3.3). There is a shift in the seasonal distribution between the two periods, with events spread more evenly throughout the year in the present period. Notably, such events - previously rare from May to September - are becoming more likely, particularly in May. This suggests that the typically summertime circulation conditions are continuing later into autumn.

We can assess the difference in the fields of composites, for both the analogue circulation variable (Z500) and meteorological hazards (rainfall and temperature). There is a deepening of the low pressure system to the northwest, which is statistically significant (Fig. 3.4 d). This increase in gradient across the region would lead to conditions conducive to more extreme rainfall in the region where the event occurred. The composites of analogue rainfall show little rainfall - as within the analogues rainfall may occur in different locations(Fig. 3.4 f-g). The difference between the two rainfall composites shows an increase in rainfall in the present period along the coast north of the impacted area, though not statistically significant (Fig. 3.4 h).

We also assess the change in annual frequency of the most similar events (Fig. 3.5). In the most similar 5% and 10% of events there is no detectable trend through time. Multidecadal variability is apparent, with an increase in frequency shown in the 1980s, and an increasing trend over the past decade. Our results imply that climate change did not alter atmospheric circulations, but caution that this result is contingent on the variables and parameters selected here and should be explored further.

We can assess trends and variability in the circulation pattern, but that alone will not determine the magnitude of the rainfall. Not all analogues that are identified produced rainfall, and in many cases the rainfall was spatially shifted. It is also important to note that the circulation pattern of this particular event is not the only circulation pattern that could lead to extreme rainfall. Other atmospheric circulation patterns - perhaps yet unseen - could cause similar or greater rainfall.

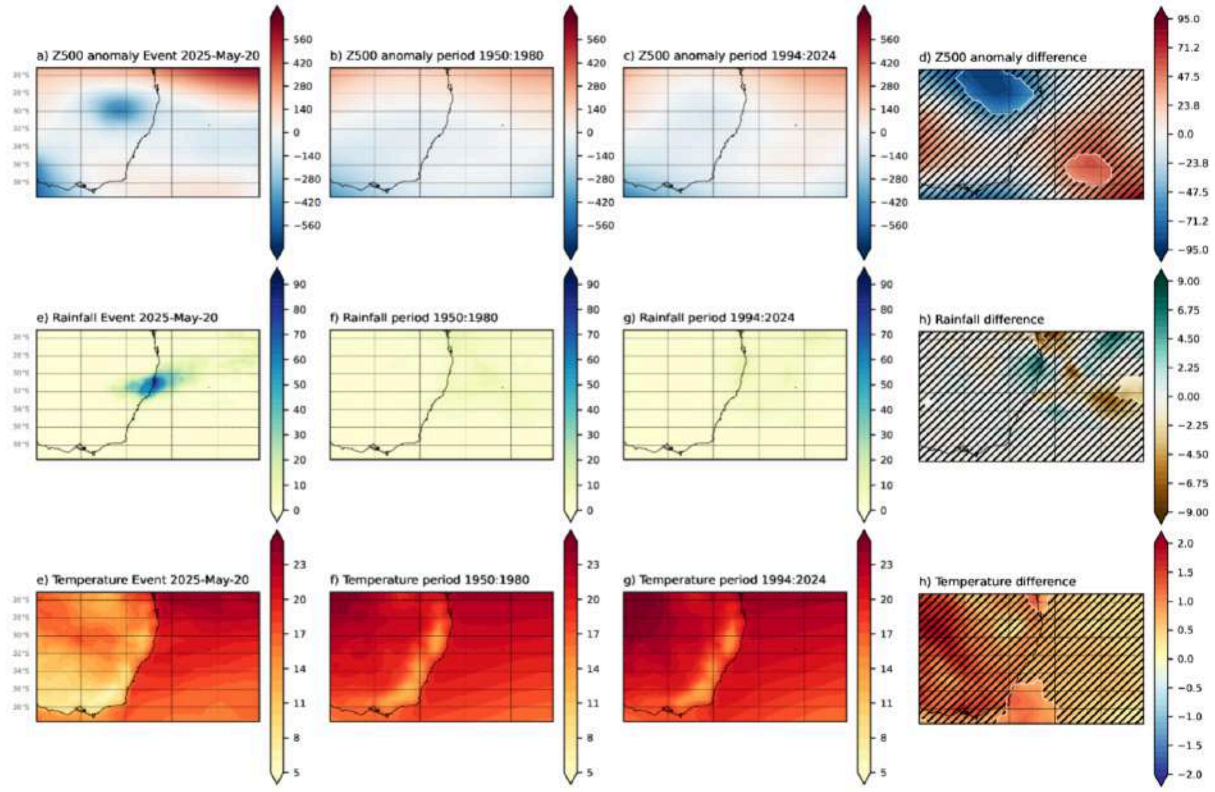

Figure 3.4: *Changes in atmospheric analogues. (a) Z500 for the event, 20th May 2025. b) Composite of the top 30 analogue days from the past period, 1950-1980. c) Composite of the top 30 analogue days from the present period, 1994-2024. d) Difference between the composites of past and present (present minus past). e-h) as in a-d for the rainfall field (mm). i-l) as in a-d for the 2m temperature field (°C). Z500 used to identify analogues in all plots. Hashing signifies regions where the signal is not significant based on a two-sided t-test.*

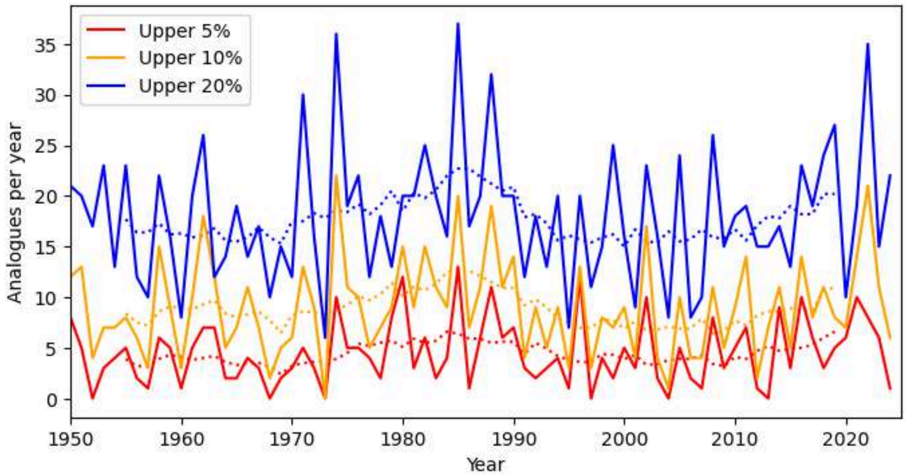

Figure 3.5: *Trends in frequency of the most similar events. Number of "good" analogues per year (in MAM) at three threshold levels: the closest 5%, 10% and 20% of most similar days (based on Euclidean distance of Z500 field. Multiannual trends (dotted lines) are plotted.*

4 Model evaluation

In this section we show the results of the model evaluation for the assessed region. The climate models are evaluated against the observations in their ability to capture:

1**. Seasonal cycles:** For this, we qualitatively compare the seasonal cycles based on model outputs against observations-based cycles . We discard the models that exhibit ill-defined peaks in their seasonal cycles. We also discard the model if the rainy season onset/termination varies significantly from the observations.

2. Spatial patterns: Models that do not match the observations in terms of the large-scale precipitation patterns are excluded.

3. **Parameters of the fitted statistical models**. We discard the model if the model and observation parameters ranges do not overlap.

The models are labelled as 'good', 'reasonable', or 'bad' based on their performance against the three evaluation criteria discussed earlier (Tables 4.1 and 4.2). A model receives an overall rating of 'good' if it is rated 'good' for all three criteria. If it is rated 'reasonable' on at least one criterion (and none are rated 'bad'), its overall rating is 'reasonable'. If it receives a 'bad' rating on any criterion, it is labelled 'bad' overall. The tables present the detailed results of the model evaluation.

The bias-corrected CORDEX models used in this study have been adjusted to match observations and consequently receive a 'good' ranking for all three criteria. However, it is important to note that this adjustment makes the comparison with the other raw model outputs uneven. The improved agreement of bias-corrected models with observations largely reflects the correction process itself, rather than an inherent improvement in their ability to simulate key processes such as rainfall trends or the underlying synoptic dynamics. Therefore, while these models perform well by the criteria applied here, this does not necessarily imply they are fundamentally better at representing physical processes relevant for rainfall extremes in the region.

In this study, a relatively large number of models were available for attribution analysis. We included those models with an overall rating of 'reasonable' or 'good'. Due to the rapid timeline of this study, the spatial evaluation was conducted only for the annual average and did not separately consider the AMJ (April–May–June) season. However, we do not expect this omission to significantly affect model selection for the AMJ case, as this season spans the end of the summer-autumn period, during which the heaviest rainfall events typically occur through to a period with fewer occurrences of this synoptic type in June, thus the AMJ period can include all synoptic situations as represented by the full year.

Table 4.1 *Evaluation results of the climate models considered for attribution analysis of AMJ RX4day. For each model, the threshold for a 1-in-10-year event is shown, along with the best estimates of the Dispersion and Shape parameters are shown, along with 95% confidence intervals. Furthermore evaluation of the seasonal cycle and spatial pattern are shown in the appendix.*

Model / Observations	Seasonal cycle	Spatial pattern	Dispersion	Shape parameter	Statistical properties	Conclusion
AWAP			0.545 (0.489 ... 0.594)	0.051 (-0.21 ... 0.25)		
ERA5			0.527 (0.443 ... 0.588)	0.042 (-0.36 ... 0.27)		
MSWEP			0.546 (0.420 ... 0.636)	0.13 (-0.26 ... 0.43)		
CPC			0.524 (0.399 ... 0.606)	0.029 (-0.40 ... 0.34)		
ACS_ACCESS-CM2_r4i1p1f1_BARPA-R ()	good	good	0.529 (0.431 ... 0.615)	0.041 (-0.12 ... 0.20)	good	good (Y)
ACS_ACCESS-CM2_r4i1p1f1_CCAM-v2203-SN ()	good	good	0.465 (0.378 ... 0.532)	-0.055 (-0.22 ... 0.11)	good	good (Y)
ACS_ACCESS-ESM1-5_r6i1p1f1_BARPA-R ()	good	good	0.565 (0.457 ... 0.653)	0.084 (-0.11 ... 0.25)	good	good (Y)
ACS_ACCESS-ESM1-5_r6i1p1f1_CCAM-v2203-SN ()	good	good	0.423 (0.331 ... 0.480)	-0.028 (-0.16 ... 0.20)	good	good (Y)
ACS_CESM2_r11i1p1f1_BARPA-R ()	good	good	0.603 (0.487 ... 0.686)	0.26 (0.086 ... 0.49)	good	good (Y)
ACS_CESM2_r11i1p1f1_CCAM-v2203-SN ()	good	good	0.575 (0.486 ... 0.646)	0.24 (0.0044 ... 0.47)	good	good (Y)
ACS_CMCC-ESM2_r1i1p1f1_BARPA-R ()	good	good	0.572 (0.459 ... 0.650)	0.33 (0.14 ... 0.60)	good	good (Y)
ACS_CMCC-ESM2_r1i1p1f1_CCAM-v2203-SN	good	good	0.412 (0.332 ... 0.473)	0.23 (0.023 ... 0.41)	good	good (Y)

()						
ACS_CNRM-ESM2-1_r1i1p1f2_CCAM-v2203-SN ()	good	good	0.489 (0.407 ... 0.551)	0.021 (-0.36 ... 0.24)	good	good (Y)
ACS_EC-Earth3_r1i1p1f1_BARPA-R ()	good	good	0.547 (0.455 ... 0.613)	0.17 (-0.12 ... 0.44)	good	good (Y)
ACS_EC-Earth3_r1i1p1f1_CCAM-v2203-SN ()	good	good	0.422 (0.349 ... 0.491)	0.23 (-0.016 ... 0.45)	good	good (Y)
ACS_MPI-ESM1-2-HR_r1i1p1f1_BARPA-R ()	good	good	0.558 (0.475 ... 0.632)	0.29 (-0.12 ... 0.57)	good	good (Y)
ACS_NorESM2-MM_r1i1p1f1_BARPA-R ()	good	good	0.557 (0.456 ... 0.638)	0.13 (-0.070 ... 0.29)	good	good (Y)
ACS_NorESM2-MM_r1i1p1f1_CCAM-v2203-SN ()	good	good	0.544 (0.432 ... 0.632)	0.17 (-0.057 ... 0.35)	good	good (Y)
CORDEX						
AUS-22_HadGEM2-ES_r1i1p1_CCLM5-0-15 ()	reasonable	good	0.617 (0.515 ... 0.698)	0.081 (-0.11 ... 0.25)	good	reasonable
AUS-22_MPI-ESM-LR_r1i1p1_CCLM5-0-15 ()	reasonable	good	0.764 (0.659 ... 0.832)	0.21 (-0.096 ... 0.67)	bad (shape good)	bad
AUS-22_NorESM1-M_r1i1p1_CCLM5-0-15 ()	reasonable	good	0.577 (0.488 ... 0.638)	0.22 (-0.028 ... 0.48)	good	reasonable
AUS-44_EC-EARTH_r12i1p1_CCLM4-8-17-CLM3-5 ()	bad	good	0.625 (0.533 ... 0.689)	0.17 (-0.11 ... 0.44)	good	bad
AUS-44_MPI-ESM-LR_r1i1p1_CCLM4-8-17-CLM3-5 ()	bad	good	0.716 (0.608 ... 0.788)	0.14 (-0.18 ... 0.58)	reasonable (shape good)	bad
HIGHRESMIP						
highresSST_CMCC-CM2-HR4_r1i1p1f1 ()	reasonable	reasonable	0.413 (0.334 ... 0.464)	-0.017 (-0.19 ... 0.28)	good	reasonable
highresSST_CMCC-CM2-VHR4_r1i1p1f1 ()	reasonable	reasonable	0.416 (0.357 ... 0.461)	0.20 (-0.040 ... 0.44)	good	reasonable
highresSST_CNRM-CM6-1_r1i1p1f2 ()	bad	good	0.513 (0.432 ... 0.572)	-0.033 (-0.20 ... 0.16)	good	bad
highresSST_CNRM-CM6-1-HR_r1i1p1f2 ()	bad	good	0.484 (0.407 ... 0.560)	-0.070 (-0.28 ... 0.094)	good	bad
highresSST_EC-Earth3P-HR_r1i1p1f1 ()	reasonable	good	0.605 (0.517 ... 0.681)	0.12 (-0.096 ... 0.31)	good	reasonable

highresSST_HadGEM3-GC31-HM_r1i1p1f1 ()	reasonable	good	0.602 (0.515 ... 0.663)	0.17 (-0.055 ... 0.40)	good	reasonable
highresSST_HadGEM3-GC31-LM_r1i14p1f1 ()	reasonable	good	0.497 (0.418 ... 0.557)	0.17 (-0.047 ... 0.35)	good	reasonable
highresSST_HadGEM3-GC31-MM_r1i1p1f1 ()	reasonable	good	0.571 (0.490 ... 0.634)	0.32 (0.035 ... 0.62)	good	reasonable
highresSST_MPI-ESM1-2-HR_r1i1p1f1 ()	reasonable	good	0.496 (0.426 ... 0.552)	-0.041 (-0.31 ... 0.20)	good	reasonable
highresSST_MPI-ESM1-2-XR_r1i1p1f1 ()	reasonable	good	0.542 (0.435 ... 0.619)	0.15 (-0.10 ... 0.45)	good	reasonable
CCAM						
CCAM-C288-NZ12km_All-Hist_r0 ()	reasonable (dry season starts a month later)	good	0.447 (0.211 ... 0.539)	0.072 (-0.14 ... 0.78)	good	reasonable
CCAM-C288-NZ12km_All-Hist_r1 ()	reasonable	good	0.413 (0.264 ... 0.492)	0.16 (-0.24 ... 0.64)	good	reasonable
CCAM-C288-NZ12km_All-Hist_r2 ()	reasonable	good	0.542 (0.344 ... 0.634)	0.10 (-0.55 ... 1.4)	good	reasonable
CCAM-C288-NZ12km_All-Hist_r3 ()	reasonable	good	0.484 (0.347 ... 0.555)	-0.27 (-0.66 ... 0.46)	good	reasonable
CCAM-C288-NZ12km_All-Hist_r4 ()	reasonable	good	0.376 (0.241 ... 0.464)	0.070 (-0.25 ... 0.51)	reasonable (shape good)	reasonable
CCAM-C288-NZ12km_All-Hist_r5 ()	reasonable	good	0.555 (0.369 ... 0.654)	0.41 (0.00060 ... 1.1)	good	reasonable
CCAM-C288-NZ12km_All-Hist_r6 ()	reasonable	good	0.464 (0.286 ... 0.549)	0.079 (-0.58 ... 0.75)	good	reasonable
CCAM-C288-NZ12km_All-Hist_r7 ()	reasonable	good	0.544 (0.345 ... 0.660)	0.048 (-0.55 ... 0.52)	good	reasonable
CCAM-C288-NZ12km_All-Hist_r8 ()	reasonable	good	0.508 (0.364 ... 0.606)	-0.23 (-0.63 ... 0.13)	good	reasonable
CCAM-C288-NZ12km_All-Hist_r9 ()	reasonable	good	0.382 (0.200 ... 0.454)	0.30 (-0.31 ... 1.9)	reasonable (shape good)	reasonable
CCAM-pooled						
CCAM-C288-NZ12km ()	reasonable	good	0.464 (0.423 ... 0.506)	0.0060 (-0.14 ... 0.15)	good	reasonable
WEATHER@HOME						

w@h50km (fact-2K) ()	reasonable	good	0.308 (0.301 ... 0.315)	-0.071 (-0.093 ... -0.051)	bad (shape good)	bad
w@h50km (fact-3K) ()	reasonable	good	0.308 (0.301 ... 0.315)	-0.071 (-0.093 ... -0.051)	Bad (shape good)	bad

Table 4.2. *Evaluation results of the climate models considered for attribution analysis of Annual (Jul-Jun) RX4day. For each model, the threshold for a 1-in-3-year event is shown, along with the best estimates of the Dispersion and Shape parameters are shown, along with 95% confidence intervals. Furthermore evaluation of the seasonal cycle and spatial pattern are shown in the appendix.*

Model / Observations	**Seasonal cycle**	**Spatial pattern**	**Dispersion**	**Shape parameter**	**Statistical properties**	**Conclusion**
AWAP			0.277 (0.239 ... 0.308)	-0.080 (-0.24 ... 0.025)		
ERA5			0.307 (0.233 ... 0.360)	-0.059 (-0.21 ... 0.14)		
MSWEP			0.263 (0.192 ... 0.318)	0.031 (-0.30 ... 0.36)		
CPC			0.274 (0.202 ... 0.322)	-0.13 (-0.46 ... 0.10)		
RCMs						
ACS_ACCESS-CM2_r4i1p1f1_BARPA-R ()	good	good	0.529 (0.431 ... 0.615)	0.041 (-0.12 ... 0.20)	bad (shape good)	bad
ACS_ACCESS-CM2_r4i1p1f1_CCAM-v2203-SN ()	good	good	0.465 (0.378 ... 0.532)	-0.055 (-0.22 ... 0.11)	bad (shape good)	bad
ACS_ACCESS-ESM1-5_r6i1p1f1_BARPA-R ()	good	good	0.565 (0.457 ... 0.653)	0.084 (-0.11 ... 0.25)	bad (shape good)	bad
ACS_ACCESS-ESM1-5_r6i1p1f1_CCAM-v2203-SN ()	good	good	0.423 (0.331 ... 0.480)	-0.028 (-0.16 ... 0.20)	reasonable (shape good)	reasonable
ACS_CESM2_r11i1p1f1_BARPA-R ()	good	good	0.603 (0.487 ... 0.686)	0.26 (0.086 ... 0.49)	bad (shape good)	bad
ACS_CESM2_r11i1p1f1_CCAM-v2203-SN ()	good	good	0.575 (0.486 ... 0.646)	0.24 (0.0044 ... 0.47)	bad (shape good)	bad
ACS_CMCC-ESM2_r1i1p1f1_BARPA-R ()	good	good	0.572 (0.459 ... 0.650)	0.33 (0.14 ... 0.60)	bad (shape good)	bad
ACS_CMCC-ESM2_r1i1p1f1_CCAM-v2203-SN ()	good	good	0.412 (0.332 ... 0.473)	0.23 (0.023 ... 0.41)	reasonable (shape good)	reasonable
ACS_CNRM-ESM2-1_r1i1p1f2_	good	good	0.489 (0.407 ... 0.551)	0.021 (-0.36 ... 0.24)	bad (shape good)	bad

CCAM-v2203-SN ()						
ACS_EC-Earth3_r1i1p1f1_BARPA-R ()	good	good	0.547 (0.455 ... 0.613)	0.17 (-0.12 ... 0.44)	bad (shape good)	bad
ACS_EC-Earth3_r1i1p1f1_CCAM-v2203-SN ()	good	good	0.422 (0.349 ... 0.491)	0.23 (-0.016 ... 0.45)	reasonable (shape good)	reasonable
ACS_MPI-ESM1-2-HR_r1i1p1f1_BARPA-R ()	good	good	0.558 (0.475 ... 0.632)	0.29 (-0.12 ... 0.57)	bad (shape good)	bad
ACS_NorESM2-MM_r1i1p1f1_BARPA-R ()	good	good	0.557 (0.456 ... 0.638)	0.13 (-0.070 ... 0.29)	bad (shape good)	bad
ACS_NorESM2-MM_r1i1p1f1_CCAM-v2203-SN ()	good	good	0.544 (0.432 ... 0.632)	0.17 (-0.057 ... 0.35)	bad (shape good)	bad
CORDEX						
AUS-22_HadGEM2-ES_r1i1p1_CCLM5-0-15 ()	reasonable	good	0.369 (0.307 ... 0.410)	0.068 (-0.16 ... 0.21)	reasonable (shape good)	reasonable
AUS-22_MPI-ESM-LR_r1i1p1_CCLM5-0-15 ()	reasonable	good	0.385 (0.312 ... 0.441)	-0.14 (-0.35 ... 0.0061)	reasonable (shape good)	reasonable
AUS-22_NorESM1-M_r1i1p1_CCLM5-0-15 ()	reasonable	good	0.354 (0.256 ... 0.415)	0.14 (-0.044 ... 0.47)	good	reasonable
AUS-44_EC-EARTH_r12i1p1_CCLM4-8-17-CLM3-5 ()	bad	good	0.322 (0.267 ... 0.363)	-0.14 (-0.40 ... 0.036)	good	bad
AUS-44_MPI-ESM-LR_r1i1p1_CCLM4-8-17-CLM3-5 ()	bad	good	0.448 (0.356 ... 0.500)	-0.15 (-0.40 ... 0.064)	reasonable (shape good)	bad
HIGHRESMIP						
highresSST_CMCC-CM2-HR4_r1i1p1f1 ()	reasonable	reasonable	0.413 (0.334 ... 0.464)	-0.017 (-0.19 ... 0.28)	reasonable (shape good)	reasonable
highresSST_CMCC-CM2-VHR4_r1i1p1f1 ()	reasonable	reasonable	0.416 (0.357 ... 0.461)	0.20 (-0.040 ... 0.44)	reasonable (shape good)	reasonable
highresSST_CNRM-CM6-1_r1i1p1f2 ()	bad	good	0.513 (0.432 ... 0.572)	-0.033 (-0.20 ... 0.16)	bad (shape good)	bad
highresSST_CNRM-CM6-1-HR_r1i1p1f2 ()	bad	good	0.484 (0.407 ... 0.560)	-0.070 (-0.28 ... 0.094)	bad (shape good)	bad
highresSST_EC-Earth3P-HR_r1i1p1f1 ()	reasonable	good	0.605 (0.517 ... 0.681)	0.12 (-0.096 ... 0.31)	bad (shape good)	bad
highresSST_HadGEM3-GC31-HM_r1i1p1f1 ()	reasonable	good	0.602 (0.515 ... 0.663)	0.17 (-0.055 ... 0.40)	bad (shape good)	bad

highresSST_HadGEM3-GC31-LM_r1i14p1f1 ()	reasonable	good	0.497 (0.418 ... 0.557)	0.17 (-0.047 ... 0.35)	bad (shape good)	bad
highresSST_HadGEM3-GC31-MM_r1i1p1f1 ()	reasonable	good	0.571 (0.490 ... 0.634)	0.32 (0.035 ... 0.62)	bad (shape good)	bad
highresSST_MPI-ESM1-2-HR_r1i1p1f1 ()	reasonable	good	0.496 (0.426 ... 0.552)	-0.041 (-0.31 ... 0.20)	bad (shape good)	bad
highresSST_MPI-ESM1-2-XR_r1i1p1f1 ()	reasonable	good	0.542 (0.435 ... 0.619)	0.15 (-0.10 ... 0.45)	bad (shape good)	bad
CCAM						
CCAM-C288-NZ 12km_All-Hist_r0 ()	reasonable (dry season starts a month later)	good	0.437 (0.274 ... 0.529)	0.053 (-0.44 ... 0.63)	reasonable (shape good)	reasonable
CCAM-C288-NZ 12km_All-Hist_r1 ()	reasonable	good	0.354 (0.230 ... 0.445)	-0.24 (-0.59 ... 0.050)	good	reasonable
CCAM-C288-NZ 12km_All-Hist_r2 ()	reasonable	good	0.367 (0.246 ... 0.442)	-0.16 (-0.51 ... 0.25)	reasonable (shape good)	reasonable
CCAM-C288-NZ 12km_All-Hist_r3 ()	reasonable	good	0.344 (0.250 ... 0.415)	-0.10 (-0.43 ... 0.31)	good	reasonable
CCAM-C288-NZ 12km_All-Hist_r4 ()	reasonable	good	0.290 (0.188 ... 0.371)	-0.017 (-0.41 ... 0.35)	good	reasonable
CCAM-C288-NZ 12km_All-Hist_r5 ()	reasonable	good	0.337 (0.211 ... 0.418)	-0.043 (-0.26 ... 0.47)	good	reasonable
CCAM-C288-NZ 12km_All-Hist_r6 ()	reasonable	good	0.345 (0.217 ... 0.421)	0.099 (-0.18 ... 0.64)	good	reasonable
CCAM-C288-NZ 12km_All-Hist_r7 ()	reasonable	good	0.395 (0.278 ... 0.475)	-0.38 (-0.82 ... 0.19)	reasonable (shape good)	reasonable
CCAM-C288-NZ 12km_All-Hist_r8 ()	reasonable	good	0.262 (0.184 ... 0.320)	0.046 (-0.30 ... 0.51)	good	reasonable
CCAM-C288-NZ 12km_All-Hist_r9 ()	reasonable	good	0.421 (0.285 ... 0.505)	-0.093 (-0.47 ... 0.43)	reasonable (shape good)	reasonable
CCAM-pooled						
CCAM-C288-NZ 12km (9)	reasonable	good	0.379 (0.337 ... 0.421)	-0.020 (-0.12 ... 0.074)	bad (shape good)	reasonable
WEATHER@HOME						
w@h50km (fact-3K) ()	reasonable	good	0.238 (0.232 ... 0.244)	-0.0060 (-0.028 ... 0.017)	good	reasonable

w@h50km (fact-2K) ()	reasonable	good	0.238 (0.232 ... 0.244)	-0.0060 (-0.028 ... 0.017)	good	reasonable

5 Multi-method multi-model attribution

This section shows Probability Ratios and change in intensity ΔI for models that passed model evaluation and also includes the values calculated from the fits with observations.

5.1 Annual (July-June) Rx4day

Table 5.1. *Event magnitude, Probability ratio and change in intensity for 3-year annual (July-Jun) Rx4day rainfall over the observational datasets and each model that passed the evaluation tests. (a) from pre-industrial climate to the present and (b) from the present to 2.6℃ above pre-industrial climate.*

		(a) Current warming level [1.3 ˚C]		(b) Future warming level [2.6 ˚C]	
Model / Observations	**Threshold for return period 3 yr**	**Probability ratio PR [-]**	**Change in intensity ΔI [mm/4day]**	**Probability ratio PR [-]**	**Change in intensity ΔI [%]**
AWAP	109.01 mm/4day	1.7 (0.84 ... 3.3)	16 (-4.2 ... 39)		
ERA5	92.855 mm/4day	1.8 (0.50 ... 6.6)	17 (-15 ... 60)		
CPC	73.435 mm/4day	1.1 (0.56 ... 2.4)	6.8 (-36 ... 68)		
ACS_ACCESS-ESM1-5_r6i1p1f1_CCAM-v2203-SN ()	1.1e+2 mm/4day	1.5 (0.88 ... 5.1)	8.3 (-2.9 ... 30)	0.77 (0.66 ... 1.0)	-8.0 (-13 ... 0.21)
ACS_CMCC-ESM2_r1i1p1f1_CCAM-v2203-SN ()	91 mm/4day	0.87 (0.71 ... 0.92)	-4.5 (-9.8 ... -2.1)	1.2 (0.91 ... 1.7)	7.0 (-3.8 ... 17)
ACS_EC-Earth3_r1i1p1f1_CCAM-v2203-SN ()	1.2e+2 mm/4day	1.9 (0.92 ... 4.1)	23 (-3.1 ... 45)	1.1 (0.80 ... 1.5)	3.0 (-5.4 ... 13)
AUS-22_HadGEM2-ES_r1i1p1_CCLM5-0-15 ()	86 mm/4day	0.86 (0.51 ... 1.7)	-5.4 (-26 ... 18)	0.79 (0.54 ... 1.1)	-8.5 (-22 ... 4.7)
AUS-22_MPI-ESM-LR_r1i1p1_CCLM5-0-15 ()	80 mm/4day	0.60 (0.41 ... 1.1)	-18 (-37 ... 1.9)	0.62 (0.27 ... 1.0)	-16 (-40 ... 1.1)

AUS-22_NorESM1-M_r1i1p1_CCLM5-0-15 ()	61 mm/4day	0.66 (0.37 ... 1.7)	-16 (-42 ... 19)	0.80 (0.43 ... 1.3)	-8.0 (-32 ... 9.4)
AUS-44_EC-EARTH_r12i1p1_CCLM4-8-17-CLM3-5 ()	2.1e+3 mm/4day	1.2 (0.51 ... 1.5)	4.6 (-22 ... 11)	0.80 (0.46 ... 1.2)	-5.8 (-20 ... 5.8)
AUS-44_MPI-ESM-LR_r1i1p1_CCLM4-8-17-CLM3-5 ()	2.3e+3 mm/4day	1.0 (0.43 ... 1.3)	1.4 (-38 ... 8.3)	0.61 (0.17 ... 0.95)	-15 (-48 ... -1.5)
highresSST_CMCC-CM2-HR4_r1i1p1f1 ()	65 mm/4day	1.4 (0.86 ... 2.9)	13 (-5.7 ... 33)	0.88 (0.76 ... 1.3)	-4.6 (-10 ... 9.0)
highresSST_CMCC-CM2-VHR4_r1i1p1f1 ()	58 mm/4day	0.93 (0.81 ... 1.4)	-3.0 (-9.5 ... 11)	0.94 (0.79 ... 1.4)	-2.8 (-11 ... 14)
CCAM-C288-NZ12km_All-Hist_r0 ()	1.3e+2 mm/4day	0.87 (0.35 ... 11)	-5.6 (-59 ... 60)	(...)	(...)
CCAM-C288-NZ12km_All-Hist_r1 ()	1.3e+2 mm/4day	0.65 (0.35 ... 14)	-14 (-54 ... 47)	(...)	(...)
CCAM-C288-NZ12km_All-Hist_r2 ()	1.2e+2 mm/4day	0.68 (0.36 ... 1.5e+2)	-13 (-53 ... 62)	(...)	(...)
CCAM-C288-NZ12km_All-Hist_r3 ()	1.7e+2 mm/4day	1.6 (0.41 ... 1.8e+2)	16 (-41 ... 1.0e+2)	(...)	(...)
CCAM-C288-NZ12km_All-Hist_r4 ()	1.2e+2 mm/4day	1.0 (0.36 ... 8.3)	0.90 (-43 ... 58)	(...)	(...)
CCAM-C288-NZ12km_All-Hist_r5 ()	1.3e+2 mm/4day	0.91 (0.36 ... 10)	-2.9 (-49 ... 56)	(...)	(...)
CCAM-C288-NZ12km_All-Hist_r6 ()	1.0e+2 mm/4day	0.40 (0.33 ... 2.2)	-41 (-76 ... 36)	(...)	(...)
CCAM-C288-NZ12km_All-Hist_r7 ()	1.1e+2 mm/4day	0.55 (0.35 ... 3.3)	-23 (-64 ... 31)	(...)	(...)
CCAM-C288-NZ12km_All-Hist_r8 ()	1.5e+2 mm/4day	2.7 (0.64 ... 62)	26 (-12 ... 1.1e+2)	(...)	(...)
CCAM-C288-NZ12km_All-Hist_r9 ()	1.5e+2 mm/4day	1.2 (0.39 ... 31)	7.0 (-46 ... 71)	(...)	(...)
CCAM-C288-NZ12km (9)	1.4e+2 mm/4day	0.83 (0.66 ... 1.1)	-5.7 (-13 ... 2.3)	0.91 (0.67 ... 1.2)	-0.026 (-0.10 ... 0.065)
w@h50km (fact-2K) ()	60 mm/4day	(...)	(...)	1.1 (1.0 ... 1.1)	0.014 (0.0010 ... 0.028)

5.2 Seasonal (AMJ) Rx4day

Table 5.2. *Probability ratio and change in intensity for 10-year AMJ Rx4day rainfall over the observational datasets and each model that passed the evaluation tests. (a) from pre-industrial climate to the present and (b) from the present to 2.6℃ above pre-industrial climate.*

Model / Observations	Threshold for return period 10 yr	Current warming level [1.3 ˚C]		Future warming level [2.6 ˚C]	
		Probability ratio PR	Change in intensity ΔI [%]	Probability ratio PR [-]	Change in intensity ΔI [%]
AWAP	109.01 mm/4day	0.89 (0.16 ... 3.4)	-3.2 (-35 ... 40)		
MSWEP	99.31 mm/4day	0.51 (0.024 ... 6.5)	-21 (-71 ... 79)		
CPC	73.435 mm/4day	0.47 (0.051 ... 2.9)	-27 (-68 ... 50)		
ACS_ACCESS-CM2_r4i1p1f1_BARPA-R ()	1.1e+2 mm/4day	0.91 (0.73 ... 1.5)	-2.6 (-8.3 ... 9.2)	0.87 (0.71 ... 1.3)	-3.9 (-9.9 ... 6.5)
ACS_ACCESS-CM2_r4i1p1f1_CCAM-v2203-SN ()	1.0e+2 mm/4day	0.92 (0.72 ... 2.5)	-1.9 (-7.3 ... 18)	1.5 (0.92 ... 2.1)	8.6 (-1.9 ... 16)
ACS_ACCESS-ESM1-5_r6i1p1f1_BARPA-R ()	1.1e+2 mm/4day	0.91 (0.80 ... 1.3)	-2.8 (-6.0 ... 8.0)	0.83 (0.69 ... 1.1)	-6.1 (-12 ... 2.7)
ACS_ACCESS-ESM1-5_r6i1p1f1_CCAM-v2203-SN ()	1.1e+2 mm/4day	1.5 (0.88 ... 5.1)	8.3 (-2.9 ... 30)	0.77 (0.66 ... 1.0)	-8.0 (-13 ... 0.21)
ACS_CESM2_r11i1p1f1_BARPA-R ()	1.1e+2 mm/4day	0.91 (0.90 ... 2.6)	-3.9 (-4.5 ... 37)	1.1 (0.83 ... 1.7)	3.2 (-7.0 ... 18)
ACS_CESM2_r11i1p1f1_CCAM-v2203-SN ()	1.1e+2 mm/4day	0.91 (0.91 ... 2.2)	-3.6 (-4.7 ... 32)	1.1 (0.85 ... 1.6)	3.4 (-6.5 ... 18)
ACS_CMCC-ESM2_r1i1p1f1_BARPA-R ()	1.0e+2 mm/4day	0.89 (0.79 ... 0.98)	-4.8 (-8.6 ... -1.2)	0.91 (0.77 ... 1.3)	-3.9 (-9.9 ... 12)
ACS_CMCC-ESM2_r1i1p1f1_CCAM-v2203-SN ()	91 mm/4day	0.87 (0.71 ... 0.92)	-4.5 (-9.8 ... -2.1)	1.2 (0.91 ... 1.7)	7.0 (-3.8 ... 17)
ACS_CNRM-ESM2-1_r1i1p1f2_CCAM-v2203-SN ()	1.0e+2 mm/4day	0.91 (0.83 ... 5.1)	-2.3 (-5.2 ... 24)	0.91 (0.69 ... 1.5)	-2.1 (-7.3 ... 8.8)
ACS_EC-Earth3_r1i1p1f1_BARPA-R ()	1.2e+2 mm/4day	1.0 (0.82 ... 1.8)	0.69 (-6.1 ... 19)	0.80 (0.67 ... 0.91)	-9.2 (-17 ... -3.5)
ACS_EC-Earth3_r1i1p1f1_CCAM-v2203-SN ()	1.2e+2 mm/4day	1.9 (0.92 ... 4.1)	23 (-3.1 ... 45)	1.1 (0.80 ... 1.5)	3.0 (-5.4 ... 13)
ACS_MPI-ESM1-2-HR_r1i1p1f1_BARPA-R ()	1.3e+2 mm/4day	1.3 (0.91 ... 1.9)	11 (-4.3 ... 28)	0.95 (0.82 ... 1.7)	-1.8 (-7.5 ... 19)

ACS_NorESM2-MM_r1i1p1f1_BARPA-R ()	1.0e+2 mm/4day	0.91 (0.75 ... 0.94)	-3.2 (-8.4 ... -1.6)	0.90 (0.71 ... 1.3)	-3.7 (-13 ... 7.6)
ACS_NorESM2-MM_r1i1p1f1_CCAM-v2203-SN ()	1.1e+2 mm/4day	0.86 (0.73 ... 0.91)	-4.9 (-9.4 ... -2.2)	0.85 (0.69 ... 0.93)	-5.2 (-12 ... -1.6)
AUS-22_HadGEM2-ES_r1i1p1_CCLM5-0-15 ()	88 mm/4day	0.51 (0.22 ... 1.7)	-21 (-49 ... 17)	0.53 (0.23 ... 1.1)	-22 (-51 ... 2.2)
AUS-22_NorESM1-M_r1i1p1_CCLM5-0-15 ()	51 mm/4day	0.58 (0.19 ... 3.2)	-20 (-57 ... 43)	1.8 (0.93 ... 3.4)	21 (-2.7 ... 39)
highresSST_CMCC-CM2-HR4_r1i1p1f1 ()	65 mm/4day	1.4 (0.86 ... 2.9)	13 (-5.7 ... 33)	0.88 (0.76 ... 1.3)	-4.6 (-10 ... 9.0)
highresSST_CMCC-CM2-VHR4_r1i1p1f1 ()	58 mm/4day	0.93 (0.81 ... 1.4)	-3.0 (-9.5 ... 11)	0.94 (0.79 ... 1.4)	-2.8 (-11 ... 14)
highresSST_EC-Earth3P-HR_r1i1p1f1 ()	93 mm/4day	0.95 (0.87 ... 2.4)	-1.6 (-4.7 ... 26)	0.86 (0.69 ... 1.1)	-5.4 (-13 ... 2.7)
highresSST_HadGEM3-GC31-HM_r1i1p1f1 ()	85 mm/4day	0.98 (0.91 ... 3.6)	-0.83 (-4.3 ... 44)	1.5 (0.90 ... 2.4)	14 (-4.8 ... 30)
highresSST_HadGEM3-GC31-LM_r1i14p1f1 ()	66 mm/4day	0.81 (0.69 ... 0.91)	-6.5 (-11 ... -2.2)	0.77 (0.66 ... 1.2)	-8.3 (-13 ... 4.9)
highresSST_HadGEM3-GC31-MM_r1i1p1f1 ()	88 mm/4day	0.91 (0.82 ... 1.6)	-4.1 (-6.7 ... 19)	0.91 (0.74 ... 1.5)	-4.1 (-11 ... 17)
highresSST_MPI-ESM1-2-HR_r1i1p1f1 ()	77 mm/4day	2.3 (0.86 ... 72)	18 (-3.8 ... 39)	1.2 (0.75 ... 2.3)	4.9 (-7.8 ... 22)
highresSST_MPI-ESM1-2-XR_r1i1p1f1 ()	78 mm/4day	1.8 (0.90 ... 4.2)	19 (-4.4 ... 39)	0.91 (0.73 ... 1.7)	-3.3 (-10 ... 16)
CCAM-C288-NZ12km_All-Hist_r0 ()	1.3e+2 mm/4day	1.4 (0.13 ... 5.5e+5)	8.3 (-54 ... 1.2e+2)	(...)	(...)
CCAM-C288-NZ12km_All-Hist_r1 ()	1.2e+2 mm/4day	0.72 (0.13 ... 11)	-8.8 (-55 ... 63)	(...)	(...)
CCAM-C288-NZ12km_All-Hist_r2 ()	99 mm/4day	0.25 (0.11 ... 21)	-39 (-79 ... 70)	(...)	(...)
CCAM-C288-NZ12km_All-Hist_r3 ()	1.8e+2 mm/4day	2.4 (0.14 ... ∞)	27 (-60 ... 1.9e+2)	(...)	(...)
CCAM-C288-NZ12km_All-Hist_r4 ()	1.9e+2 mm/4day	17 (0.32 ... 8.4e+3)	1.1e+2 (-22 ... 2.8e+2)	(...)	(...)
CCAM-C288-NZ12km_All-Hist_r5 ()	1.6e+2 mm/4day	1.4 (0.15 ... 19)	16 (-66 ... 1.5e+2)	(...)	(...)
CCAM-C288-NZ12km_All-Hist_r6 ()	1.1e+2 mm/4day	0.24 (0.10 ... 4.1)	-45 (-84 ... 68)	(...)	(...)
CCAM-C288-NZ12km_All-Hist_r7 ()	1.5e+2 mm/4day	11 (0.27 ... ∞)	61 (-31 ... 2.6e+2)	(...)	(...)
CCAM-C288-NZ12km_All-Hist_r8 ()	1.5e+2 mm/4day	9.6 (0.18 ... ∞)	31 (-38 ... 1.6e+2)	(...)	(...)

CCAM-C288-NZ12km ()	1.3e+2 mm/4day	0.55 (0.38 ... 0.78)	-16 (-25 ... -6.4)	0.87 (0.50 ... 1.3)	-0.035 (-0.14 ... 0.086)

6 Hazard synthesis

For the two event definitions described above, RX4-day over AMJ and annual (Jul-Jun), we evaluate the influence of anthropogenic climate change by calculating the probability ratio as well as the change in intensity using observations and climate models. Models which do not pass the evaluation described above are excluded from the analysis. The aim is to synthesise results from models that pass the evaluation along with the observations-based products, to give an overarching attribution statement.

Figures 6.1-6.2 (and Appendix Figure A1-A2) show the summary of the changes in probability and intensity for the observations (blue) and models (red). The detailed plots showing how the individual observed datasets and climate models are combined together to get the overarching results, are shown in appendix Figures A1-A2. To account for the difference between observations-based datasets that cannot be explained by natural variability a representation error is added (in quadrature) to the observations. This is shown in these figures as white boxes around the light blue bars. The dark blue bar shows the average over the observation-based products. Next, a term to account for intermodel spread is added (in quadrature) to the natural variability of the models. This is shown in the figures as white boxes around the light red bars. The dark red bar shows the model average, consisting of a weighted mean using the (uncorrelated) uncertainties due to natural variability plus the term representing intermodel spread (i.e., the inverse square of the white bars).

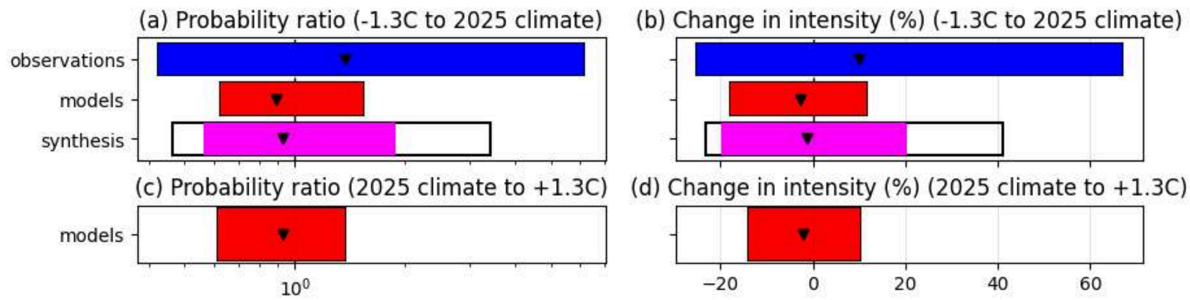

Figure 6.1: *Summary of synthesis of (a) probability ratios and (b) intensity change when comparing annual (July- June) Rx4day over the study region with a 1.3℃ cooler climate. See Appendix Fig. A1 to view these ranges for all the observed datasets and climate models that passed model valistation.*

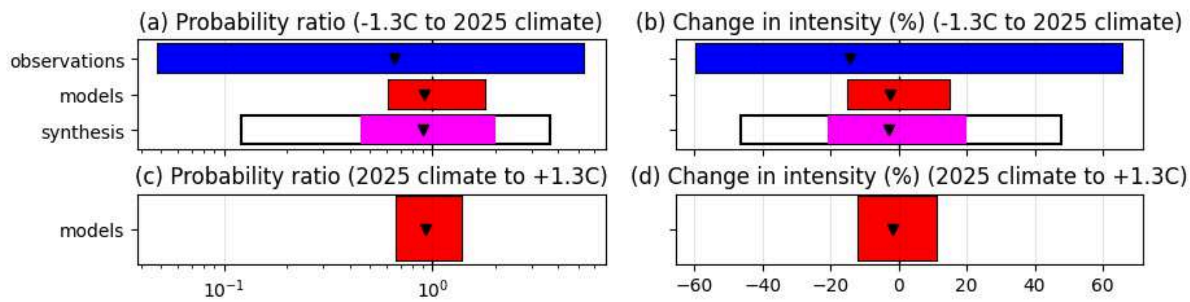

Figure 6.2: *Summary of synthesis of (a) probability ratios and (b) intensity change when comparing seasonal (AMJ) Rx4day over the study region with a 1.3℃ cooler climate. See Appendix Fig. A2 to view these ranges for all the observed datasets and climate models that passed model valistation.*

Usually, we combine observation-based products and models into a single synthesised result using two approaches (Otto et al., 2024), that are indicated by the magenta and white bars at the bottom of

Appendix Figures A1-A2. However, as can be clearly seen by the light red bars in these figures showing the individual model results, some of these are incompatible with each other. While some climate models, such as most of the CCAM models, show a decreasing trend in rainfall extremes in the region, others including some of the downscaled models under the CORDEX experiment and the downscaled and bias-corrected CMIP6 models, show an increase. In both these cases, the best-estimated changes in individual models suggest emerging trends that are larger than which could be explained by internal variability and the Clausius-Clapeyron expectation (for those models that show increasing tendency). This seemingly suggests that the circulation patterns driving heavy rainfall in the models are changing, but the extent of these changes are different in different models. These mixed trends are evident not only in the historic simulations, but also in the projections of heavy rainfall in a 2.6°C warmer climate above the preindustrial baseline. As we have employed a number of climate models that pass the evaluation criteria for this analysis, we have no means to assume some of them are more realistic than others, without a more detailed analysis of the model construction.
In contrast, the observational products, highlighted in light blue in Figures A1 and A2 are consistent with each other and indicate a trend towards an increase in the wettest 4-day event over the whole year, but a decrease in heavy rainfall over the AMJ season. The consistency in the observed trends for the RX4-day annual event is in line with the finding from the analysis of the circulation analogues associated with the event (as described in section 3.3) that saw an increase in rainfall for the wettests events. The drying observed in AMJ cannot be explained by the suggested tendency towards rainfall extremes shifting from March to May, and thus requires further study.

Overall, we thus cannot make an overarching attribution statement for the events as analysed here without further analysis. In table 6.1, summarising the results we thus only highlight the observational results, but do not suggest that the quantitative synthesis or future model assessment provide meaningful information.

The findings from this study are in line with previous studies that also found that with currently available models and observations it is difficult to identify how climate change manifests in extreme rainfall in this region that is geographically and climatically transitional. It lies between the southern area, which exhibits a clear drying trend associated with climate change in the colder months of the year, and the northern area, where rainfall trends are more mixed. Additionally, the timing of the event introduces further complexity, as the month of May marks the seasonal transition from the warmer to the cooler part of the year. This poses challenges for climate adaptation as emergency responses as well as long term planning needs to be robust for a range of possible futures that can be substantially dryer and wetter than all events observed in the historical record. With the circulation analogues (section 3.3) as well as the observations showing an increasing tendency towards heavier and more frequent rainfall extremes in the region, and research on sub-daily timescales (discussed in Section 1.1) showing a consistent increase in models, the risk of heavy rainfall spells and flooding worse than observed until now needs to be taken especially seriously.

***Table 6.1**: Summary of results for both event definitions, presented in Figs 6.1 and 6.2: changes due to GMST include past-present changes and present-future changes. We highlight consistent increases in the observations in light blue and decrease in light orange, while not highlighting any results including models as the individual models are incompatible with each other and combining them is thus not informative. The fact that combined results are close to no change should not be taken as a higher likelihood of no change compared to larger changes in individual models (Appendix Figures A1 & A2)*

Data		**Annual (Jul-Jun) rx4day**		**AMJ rx4day**	
		Probability ratio (95% CI)	**Intensity change (%) (95% CI)**	**Probability ratio (95% CI)**	**Intensity change (%) (95% CI)**
Observations	**Past-Present**	1.37 (0.425 … 6.15)	9.87 (-25.1 … 66.8)	0.651 (0.049 … 5.33)	-14.5 (-59.3 … 65.6)
Models		0.886 (0.624 … 1.54)	-2.70 (-17.8 … 11.5)	0.912 (0.619 … 1.80)	-2.41 (-14.7 … 15.1)
Synthesis		0.927 (0.561 … 1.89)	-1.19 (-19.8 … 20.2)	0.897 (0.451 … 2.01)	-2.98 (-20.8 … 20)
Models only	**Present-Future**	0.927 (0.616 … 1.37)	-1.99 (-14.0 … 10.1)	0.922 (0.670 … 1.39)	-1.85 (-11.8 … 11.2)

7 Vulnerability and Exposure

New South Wales (NSW), located in southeastern Australia, is a geographically varied state comprising coastal plains, mountainous regions, and expansive inland river systems. This diversity contributes significantly to its complex flood risk profile. The coast, including the Mid North Coast and Hunter regions, is particularly susceptible to flash flooding due to low-lying floodplains and intense rainfall events. Inland, major river systems such as the Murrumbridgee, Macquarie, and Namoi rivers render towns like Forbes, Moree, Walgett, Moama, and Narrabi highly exposed to flood risk (Groundsure ClimateIndex via Property Buzz, 2024). Coastal towns like Yamba, Grafton, and Port Macquarie are also at risk due to their proximity to river mouths and low-lying land (Ibid.). Outside of the coastal towns, populations are much more rural and spread out, increasing challenges with flood rescues.

Between 18 and 25 May 2025, NSW experienced record-breaking rainfall triggering widespread flooding, especially in the Mid North Coast and Hunter Valley. Towns such as Taree, Kempsey, and Coffs Harbour were among the hardest hit (see Figure 7). The disaster resulted in five fatalities, the days-long stranding of about 50,000 people, thousands of evacuations, and severe damage to homes, agriculture, and infrastructure (Evans & MacKenzie, 2025; Feiam & Wilcox, 2025). The Manning River at Taree surpassed a century-old flood record, exceeding six meters on 21 May, marking the event as one of the most severe in the state's recorded history (The Sydney Morning Herald, 2025). The Insurance Council of Australia (ICA) has declared this a significant event, with over 6,000 insurance claims in the Mid North Coast and Hunter regions, with the majority relating to damaged homes (ICA, 2025).

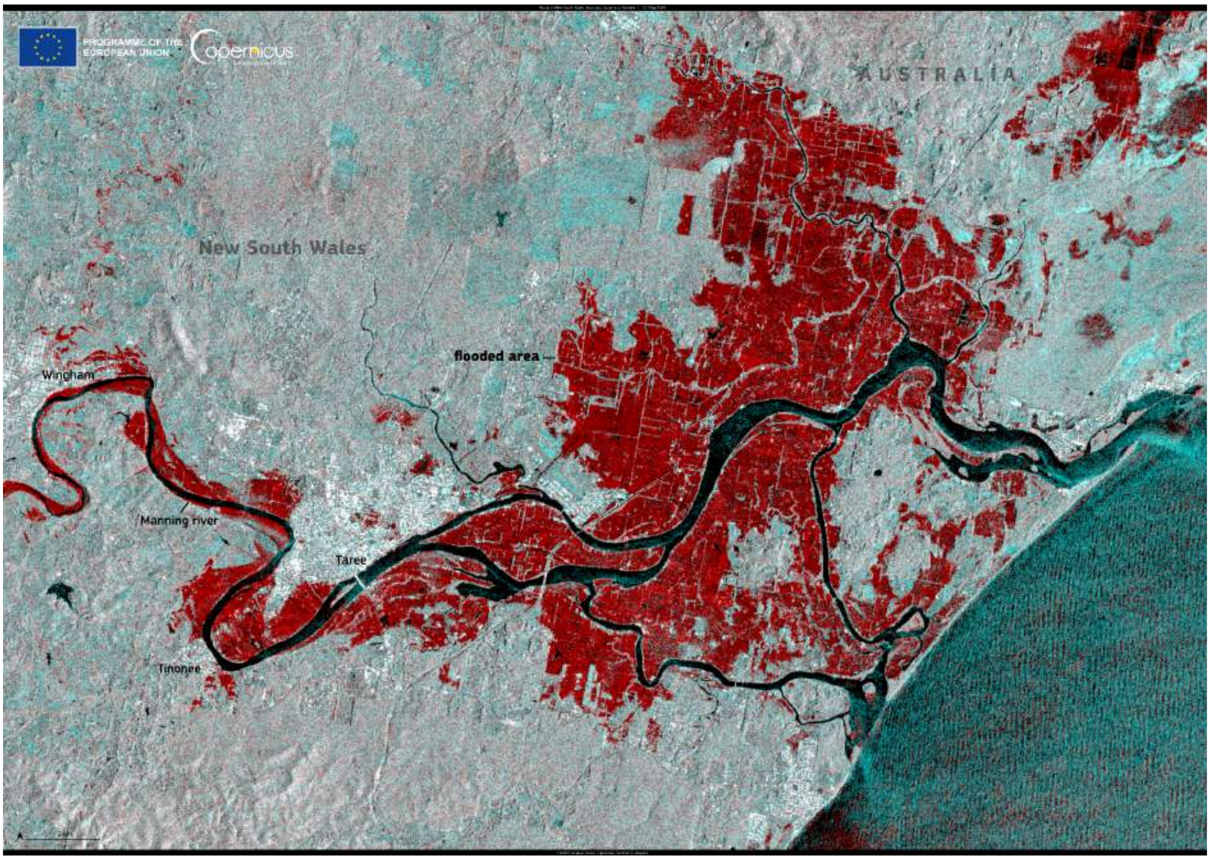

***Figure** 7: Flood extent as of 21 May in the Hunter Valley and Mid North Coast, showing that the towns of Taree and Tinonee were among the hardest-hit. Source: European Union, Copernicus Sentinel-1 imagery (2025).*

7.1 Flood risk and compounding events

NSW, Australia's most populous state, faces heightened vulnerability to flooding, particularly in the northeast where socioeconomic disadvantage and high exposure to weather extremes intersect (Sewell et al., 2015). Between 2004 and 2014, floods triggered the highest number of disaster declarations in NSW among extreme weather events, with the Northern Rivers and Mid North Coast regions in the northeast identified as disaster hotspots. Notably, 43% of the state's most socio-economically disadvantaged Local Government Areas (LGAs) fell within this zone, including the LGAs of Clarence Valley, Kempsey, Nambuca, Richmond Valley, Kyogle, and Tenterfield (Sewell et al., 2015) - the first three of which were impacted by the 2025 floods (NSW Government, 2025). Since 2014, major floods in 2017, 2021, 2022, and 2025 have surpassed previous impacts in scale and frequency.

NSW has not only experienced repeated flooding, but a range of extreme weather events over the past two decades, often affecting the same regions. Rather than isolated crises, these events reflect a compounding pattern of shocks that interact with existing vulnerabilities, placing cumulative strain on infrastructure, services, and social resilience, deepening recovery fatigue (Matthews et al., 2019; NRCF & PaperGiant, 2022).

Several major events illustrate this pattern. The 2010-2011 floods in northeastern NSW caused 33 fatalities, damaged 28,000 properties, and led to approximately $4 billion in economic losses, with widespread disruption across several key sectors like mining and agriculture (Australian Disaster Resilience Knowledge Hub, n.d.). In 2021, flooding from the North Coast to Sydney impacted 25,500 people, damaged 4,000 properties, and caused nearly $3 billion in damages (Royal Far West & UNICEF Australia, 2023). NSW also faced prolonged drought between 2017-2020, which reduced state GDP by an estimated $10.2 billion due to agricultural losses and water shortages (NSW Government, n.d.a-). The 2019-2020 bushfires destroyed over 2,100 homes and burned approximately 5.5 million hectares, leaving 25 people dead (NSW Government, n.d.-b). More recently, the 2022 floods across eastern Australia resulted in 14 deaths and displaced 15,000 people, with uninsured losses exceeding $5.65 billion (Queensland Reconstruction Authority, 2022; Royal Far West & UNICEF Australia, 2023). These events, together with recent heatwaves and the 2025 floods, underscore the systemic and overlapping nature of extreme weather events in the regions.

Flood impacts in NSW are unevenly distributed, with rural populations and residents of larger towns and smaller cities often bearing the brunt due to limited access to services and entrenched social vulnerabilities (Magdy et al., 2023). In the Mid North Coast and other affected regions, disadvantage is linked to increased flood exposure, with renters, people with disabilities, and older adults often less able to prepare, evacuate, and recover effectively (Rolfe et al., 2020). In the Mid North Coast, these vulnerabilities are partly reflected in census data from 2021: the region has a higher share of older adults than the national average (17.7% vs 17.2%) and renters (32.6% vs 30.6%), but a lower share of people reporting one or more long-term health conditions (Australian Bureau of Statistics, 2021).

Recovery from past events has been protracted and uneven. In 2022, for example, more than 3,500 homes were declared uninhabitable, and up to 20,000 people - many from already marginalized communities - were displaced for extended periods (Bennett-Levy, 2022; NRCF & PaperGiant, 2022). Residents reported confusion over recovery options, limited access to housing and mental health support, and widespread economic disruption following job losses (NRCF & PaperGiant, 2022). While not spatially overlapping, earlier examples reveal similar patterns: during the 2017 floods in Northern NSW, 82% of those severely affected in Lismore and 50% in the Tweed region were in the lowest income bracket (University of Sydney, 2022). Aboriginal and Torres Strait Islander Peoples, people with disabilities, and those on income support were significantly more likely to be displaced and face prolonged recovery (Bennett-Levy, 2022).

Building on existing progress, there is growing recognition of the need to strengthen long-term, community centered resilience to floods. This includes support for Community Land Trusts, co-designed disaster responses and regional resilience plans, and enabling locally led initiatives (University of Sydney, 2022). These approaches can also help reduce long-term mental health risks, especially for those facing repeated displacement and disadvantage.

While flood vulnerability is shaped by social and spatial dynamics, sector-specific exposure also plays a critical role. The agricultural sector in NSW exemplifies this, with recurrent impacts that reflect and reinforce systemic risk.

7.2 Agriculture

NSW has important agricultural industries, including a large share of Australia's grain, dairy production and houses a third of the country's sheep and one fifth of its cattle (Britannica, 2025). The impacts from the 2025 floods were significant with low lying farms being inundated, pasture waterlogged, and cattle drowned (The Guardian, 2025). This comes after the devastating ex-Tropical Cyclone Alfred in 2021 which some farmers were still recovering from (Ibid.). An estimated 137 dairy farms are impacted by the floods, and the impacts will likely continue longer term as many cows are now unwell or will produce less with missed milkings (ABC, 2025). Farmers are being encouraged to report damages quickly in order for the government to understand the scale of the damage and resources required for recovery (NSW Government, 2025). Prior to these floods, dairy farming was already a declining industry in the region with the number of farms declining over the last 10 years (ABC, 2025). A lack of support for floodplain agriculture, and other headwinds such as land-use conflict and increasing cost of production, are also affecting farming in the region (AdaptNSW, 2019).

Understanding risk drivers also requires examining the structures and systems designed to reduce them. Flood risk management policies and plans, and early warning systems provide crucial insights into institutional capacity.

7.3 Flood risk management

Flood risk in NSW is shaped not only by physical and social exposure, but also by the structure and effectiveness of the systems designed to reduce, anticipate, or respond to that risk. These systems span floodplain planning, hard and soft mitigation measures, early warnings, and emergency response coordination. Together, they constitute the institutional and technical infrastructure that enables - or limits- adaptive capacity at the community level.

7.3.1 Policy and planning landscape

Floodplain risk management in NSW is governed through a multi-tiered institutional framework. Local governments manage development and zoning, while the NSW Government provides technical guidance, data, and financial support for risk management plans (NSW Government, n.d.-a). The Australian Government, through the Bureau of Meteorology (BoM), coordinates climate modelling and forecasting.

The core policy framework is provided by the NSW Flood Prone Land Policy, which mandates that councils assess flood risk beyond the 1% annual exceedance probability, accounting for less frequent but more extreme events. Councils are encouraged to develop Flood Risk Management Plans, supported by risk-informed planning controls that limit new developments in high-risk areas (NSW Government, n.d.-a). This is operationalized through the Flood Risk Management Manual, structured around ten principles and supported by 14 technical and planning guidelines (NSW Government, n.d.-b). Further support is provided via the NSW Government's Floodplain Management Program, which delivers financial and technical assistance to local councils and land managers, including support for flood modelling and community engagement (NSW Government, n.d.-c). Despite comprehensive planning frameworks, gaps persist between enabling disaster recovery and managing long-term risk, as rebuilding in flood-prone areas is often permitted. In 2021, NSW introduced a new clause which allows councils to grant development consent to repair or rebuild properties damaged by natural hazards, though it would not normally comply with development standards (Local

Government NSW, 2022). Despite criticism, more than 30 councils have reportedly adopted the clause (Corrs Chambers Westgarth, 2022; The Law Society of New South Wales, 2020). Without uniform resilience mandates or relocation incentives, current practices risk perpetuating community vulnerability to future floods.

Strategic direction is also shaped by broader adaptation initiatives. The NSW Climate Change Adaptation Action Plan 2025-2029 (NSW Government, 2024) promotes integrated, cross-sector responses to climate risk, while the North Coast Enabling Regional Adaptation report (NSW Government, 2019) highlights the need for place-based responses - including natural floodplain restoration and adaptive agriculture in the Mid North Coast.

Despite progress, governance remains complex with shared responsibilities across local, state, and federal levels. Coordination can also be challenging, particularly in regions where flood risks span multiple jurisdictions, but ongoing efforts to strengthen regional collaboration and data sharing are promising. Further, recent analysis of NSW recovery planning reveals limited integration of disaster risk reduction, particularly in prevention, mitigation, and participatory mechanisms. Local plans often lack hazard identification and fail to embed resilience measures, undermining long-term adaptation - particularly concerning in flood-prone regions such as the Mid North Coast and Hunter Valley.

7.3.2 Early Warning System

The Bureau of Meteorology (BoM) issues Severe Weather Warnings, Flood Watches, and Flood Warnings based on real-time rainfall and river data, which are disseminated to the public via media, online platforms, and emergency services (BoM, n.d.). In NSW, forecasts issued by the BoM, are operationalized through the NSW State Emergency Service (SES), the lead agency for flood response and community warnings (NSW SES, n.d.).

In the case of the May 2025 floods, the SES issued an initial Flood Watch on 16 May for the Mid North Coast and Hunter regions, providing three days of lead time before the onset of the heavy rainfall on the 19th (NSW SES, 2025a). As conditions worsened, flood alerts expanded rapidly, enabling life-saving early actions. The SES prepositioned flood rescue teams, including aviation assets and vehicles, and prepared communities ahead of the floods (NSW SES, 2025b). Evacuations took place across multiple LGAs, with thousands of residents displaced following SES warnings and alerts. Orders were updated nearly hourly and targeted flood-prone suburbs, rural areas, and low-lying communities, most of which are located along the Manning, Macleay, and Bellinger rivers (NSW SES, 2025c).

Vulnerability and Exposure Conclusions

The May 2025 floods in New South Wales reflect a convergence of hazard exposure and vulnerability. Communities in flood-prone regions, particularly in the Mid North Coast, experienced disproportionate impacts due to intersecting factors such as socioeconomic marginalization, limited mobility, insecure housing, and geographic isolation. Vulnerable groups such as renters, older adults, and people with disabilities remain at heightened risk, while agricultural systems, particularly dairy and grazing, continue to face cumulative stress from compounding hazards.

In light of the differences in climate projections - with both increased rainfall and drying trends projected across models - adaptation strategies must be robust, flexible, and responsive to a range of future conditions. While Australia possesses strong institutional and technical capacity for disaster risk management, recent events reveal persistent social and geographic disparities in who is most affected. Notably, local recovery plans often overlook fundamental risk reduction measures, such as identifying hazards and embedding resilience-building strategies. This limits adaptive capacity and risks entrenching exposure in flood-prone areas like the Mid North Coast and Hunter Valley. Low-regrets adaptation measures such as water storage and distribution systems that help manage water regardless volume, nature-based solutions (e.g. wetlands and floodplain restoration), and improved risk management (e.g. early warnings and early action, insurance schemes) can be beneficial for both wet and dry extremes.

While this analysis is not exhaustive, the findings suggest that adaptation measures may benefit from greater attention to groups with limited mobility, insecure housing, or constrained recovery capacity, particularly in rural areas. Parts of the agricultural sector, especially small-scale or climate-sensitive producers, also face heightened risk under current and future conditions. Locally grounded approaches, such as adaptive land stewardship and community-led resilience planning, may offer valuable pathways for more socially responsive adaptation.

Data availability

All time series used in the attribution analysis are available via the Climate Explorer.
%FOR DATA THAT ISN'T, data is available upon request, CONTACT...:

References

All references are given as hyperlinks in the text.

Appendix

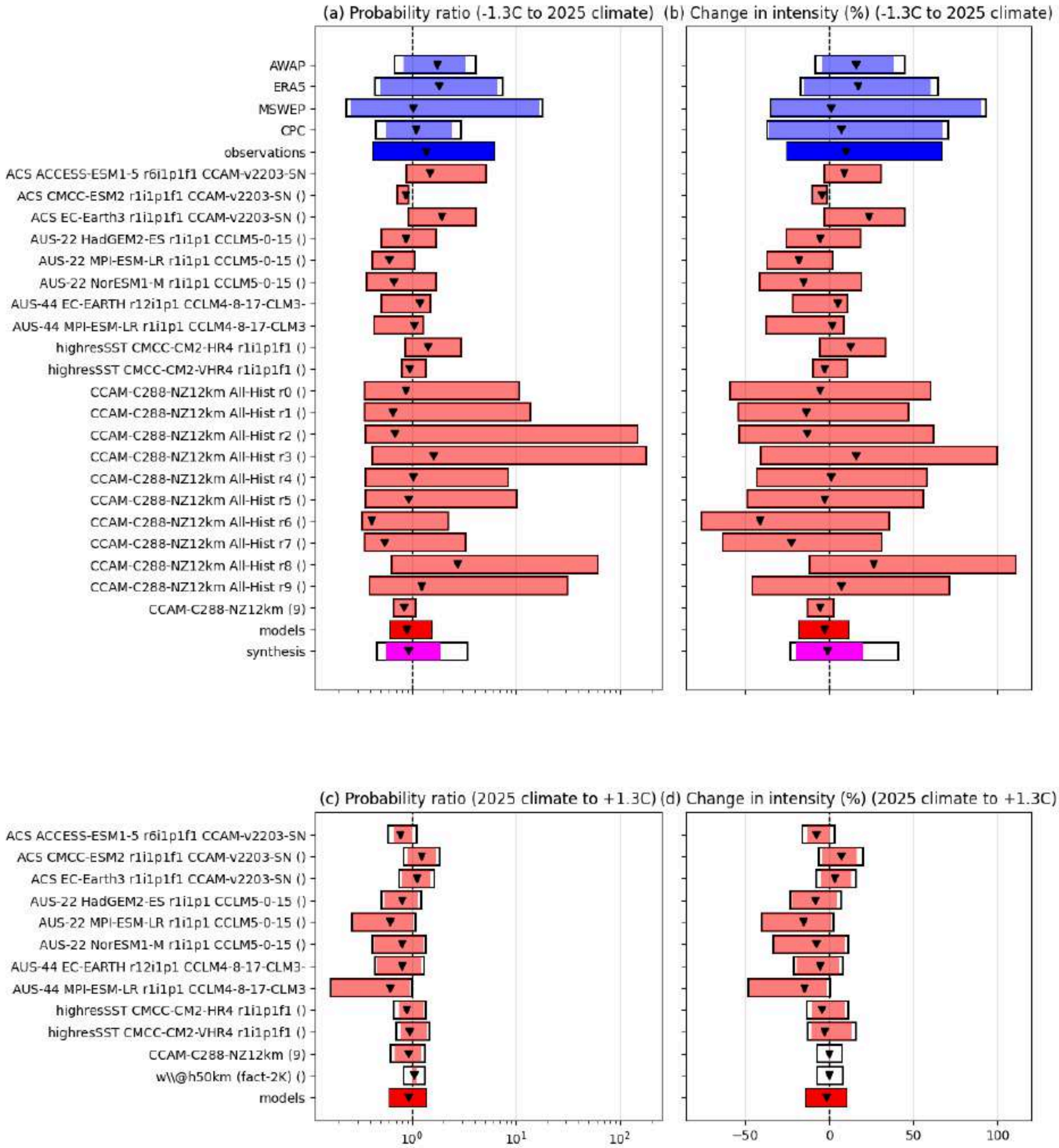

Figure A1*: Synthesis of (a) probability ratios and (b) intensity change when comparing annual (Jul-Jun) Rx4day day over the study region with a 1.3℃ cooler climate. Synthesis of c) intensity change and (d) probability ratios when comparing the event with a 1.3℃ warmer climate.*

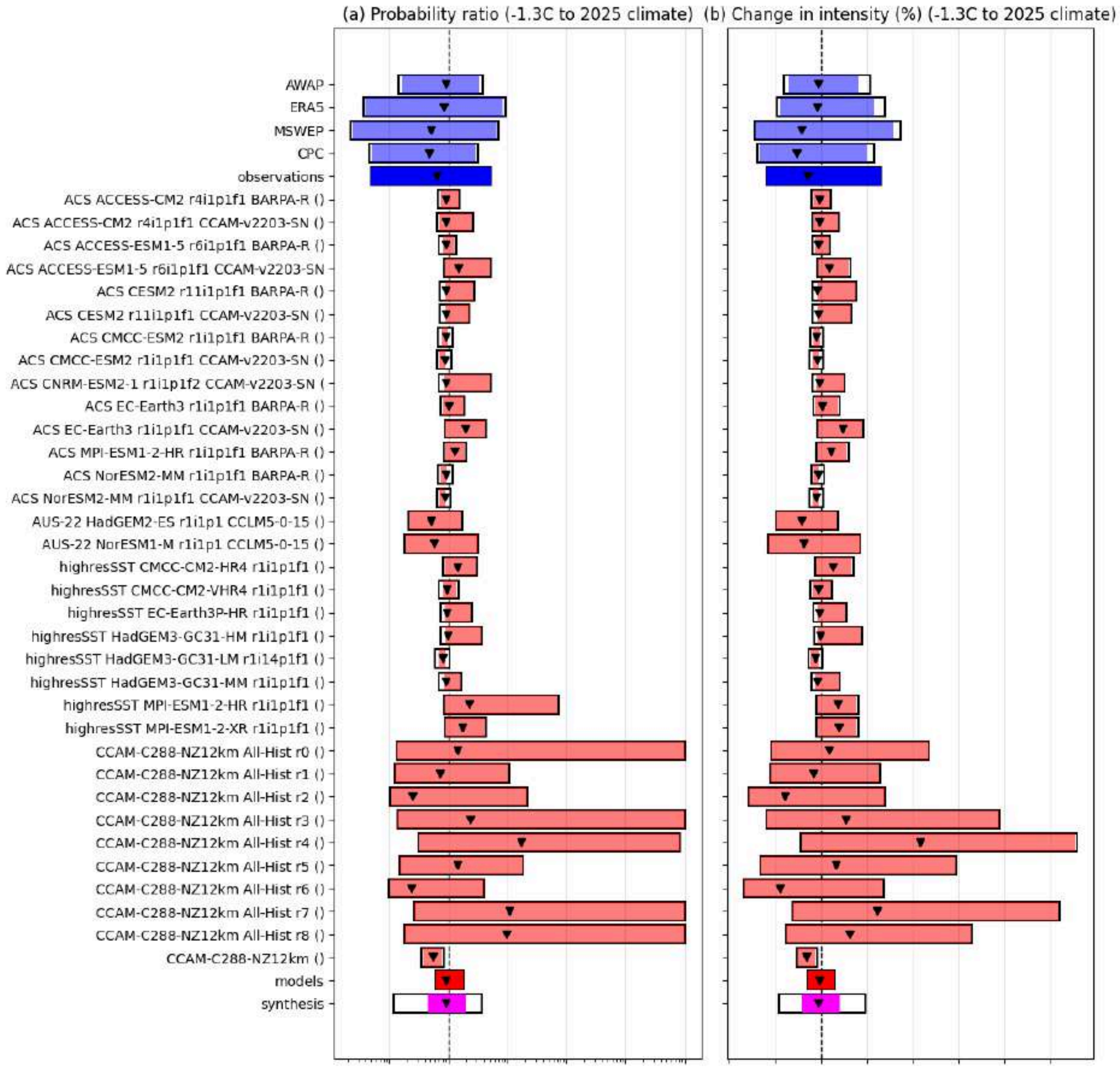

(a) Probability ratio (-1.3C to 2025 climate)
(b) Change in intensity (%) (-1.3C to 2025 climate)
AWAP
ERA5
MSWEP
CPC
observations
ACS ACCESS-CM2 r4i1p1f1 BARPA-R ()
ACS ACCESS-CM2 r4i1p1f1 CCAM-v2203-SN ()
ACS ACCESS-ESM1-5 r6i1p1f1 BARPA-R ()
ACS ACCESS-ESM1-5 r6i1p1f1 CCAM-v2203-SN
ACS CESM2 r11i1p1f1 BARPA-R ()
ACS CESM2 r11i1p1f1 CCAM-v2203-SN ()
ACS CMCC-ESM2 r1i1p1f1 BARPA-R ()
ACS CMCC-ESM2 r1i1p1f1 CCAM-v2203-SN ()
ACS CNRM-ESM2-1 r1i1p1f2 CCAM-v2203-SN (
ACS EC-Earth3 r1i1p1f1 BARPA-R ()
ACS EC-Earth3 r1i1p1f1 CCAM-v2203-SN ()
ACS MPI-ESM1-2-HR r1i1p1f1 BARPA-R ()
ACS NorESM2-MM r1i1p1f1 BARPA-R ()
ACS NorESM2-MM r1i1p1f1 CCAM-v2203-SN ()
AUS-22 HadGEM2-ES r1i1p1 CCLM5-0-15 ()
AUS-22 NorESM1-M r1i1p1 CCLM5-0-15 ()
highresSST CMCC-CM2-HR4 r1i1p1f1 ()
highresSST CMCC-CM2-VHR4 r1i1p1f1 ()
highresSST EC-Earth3P-HR r1i1p1f1 ()
highresSST HadGEM3-GC31-HM r1i1p1f1 ()
highresSST HadGEM3-GC31-LM r1i14p1f1 ()
highresSST HadGEM3-GC31-MM r1i1p1f1 ()
highresSST MPI-ESM1-2-HR r1i1p1f1 ()
highresSST MPI-ESM1-2-XR r1i1p1f1 ()
CCAM-C288-NZ12km All-Hist r0 ()
CCAM-C288-NZ12km All-Hist r1 ()
CCAM-C288-NZ12km All-Hist r2 ()
CCAM-C288-NZ12km All-Hist r3 ()
CCAM-C288-NZ12km All-Hist r4 ()
CCAM-C288-NZ12km All-Hist r5 ()
CCAM-C288-NZ12km All-Hist r6 ()
CCAM-C288-NZ12km All-Hist r7 ()
CCAM-C288-NZ12km All-Hist r8 ()
CCAM-C288-NZ12km ()
models
synthesis

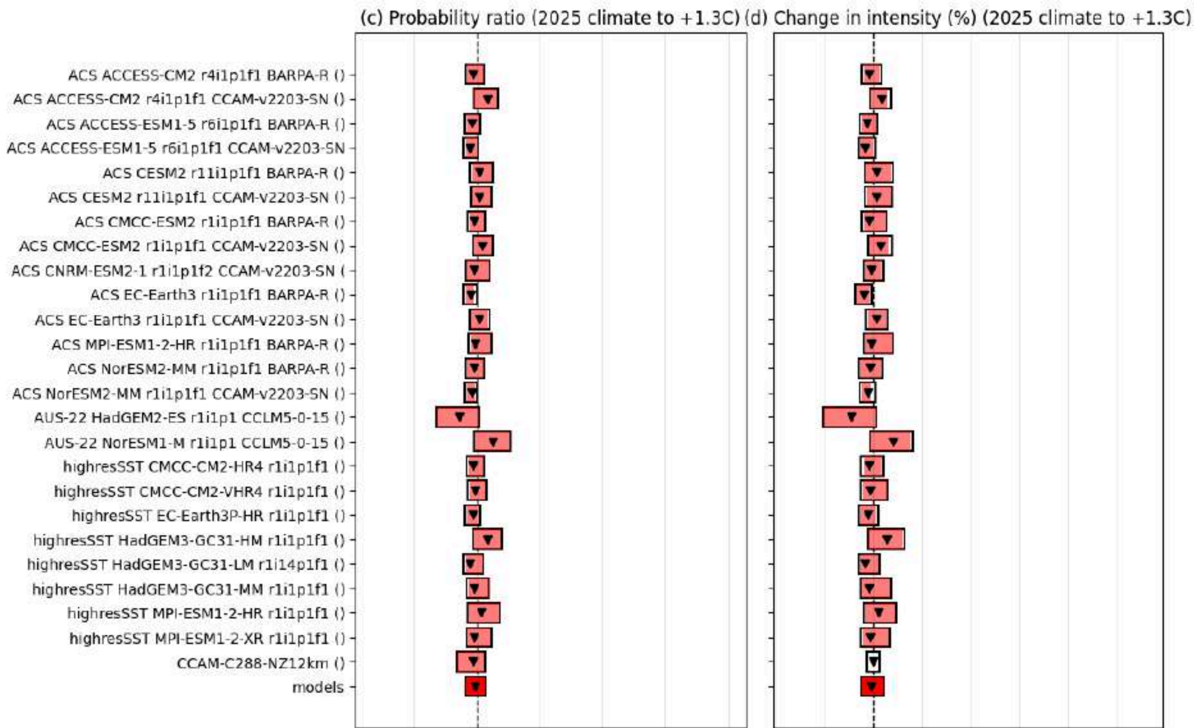

(c) Probability ratio (2025 climate to +1.3C)
(d) Change in intensity (%) (2025 climate to +1.3C)
ACS ACCESS-CM2 r4i1p1f1 BARPA-R ()
ACS ACCESS-CM2 r4i1p1f1 CCAM-v2203-SN ()
ACS ACCESS-ESM1-5 r6i1p1f1 BARPA-R ()
ACS ACCESS-ESM1-5 r6i1p1f1 CCAM-v2203-SN
ACS CESM2 r11i1p1f1 BARPA-R ()
ACS CESM2 r11i1p1f1 CCAM-v2203-SN ()
ACS CMCC-ESM2 r1i1p1f1 BARPA-R ()
ACS CMCC-ESM2 r1i1p1f1 CCAM-v2203-SN ()
ACS CNRM-ESM2-1 r1i1p1f2 CCAM-v2203-SN (
ACS EC-Earth3 r1i1p1f1 BARPA-R ()
ACS EC-Earth3 r1i1p1f1 CCAM-v2203-SN ()
ACS MPI-ESM1-2-HR r1i1p1f1 BARPA-R ()
ACS NorESM2-MM r1i1p1f1 BARPA-R ()
ACS NorESM2-MM r1i1p1f1 CCAM-v2203-SN ()
AUS-22 HadGEM2-ES r1i1p1 CCLM5-0-15 ()
AUS-22 NorESM1-M r1i1p1 CCLM5-0-15 ()
highresSST CMCC-CM2-HR4 r1i1p1f1 ()
highresSST CMCC-CM2-VHR4 r1i1p1f1 ()
highresSST EC-Earth3P-HR r1i1p1f1 ()
highresSST HadGEM3-GC31-HM r1i1p1f1 ()
highresSST HadGEM3-GC31-LM r1i14p1f1 ()
highresSST HadGEM3-GC31-MM r1i1p1f1 ()
highresSST MPI-ESM1-2-HR r1i1p1f1 ()
highresSST MPI-ESM1-2-XR r1i1p1f1 ()
CCAM-C288-NZ12km ()
models

Figure A2*: Synthesis of (a)probability ratios and (b) intensity change when comparing seasonal (AMJ) Rx4day day over the study region with a 1.3*℃ *cooler climate. Synthesis of c) intensity change and (d) probability ratios when comparing the event with a 1.3*℃ *warmer climate.*